Cancer Cell

Article

Taxanes trigger cancer cell killing *in vivo* by inducing non-canonical T cell cytotoxicity

Graphical abstract

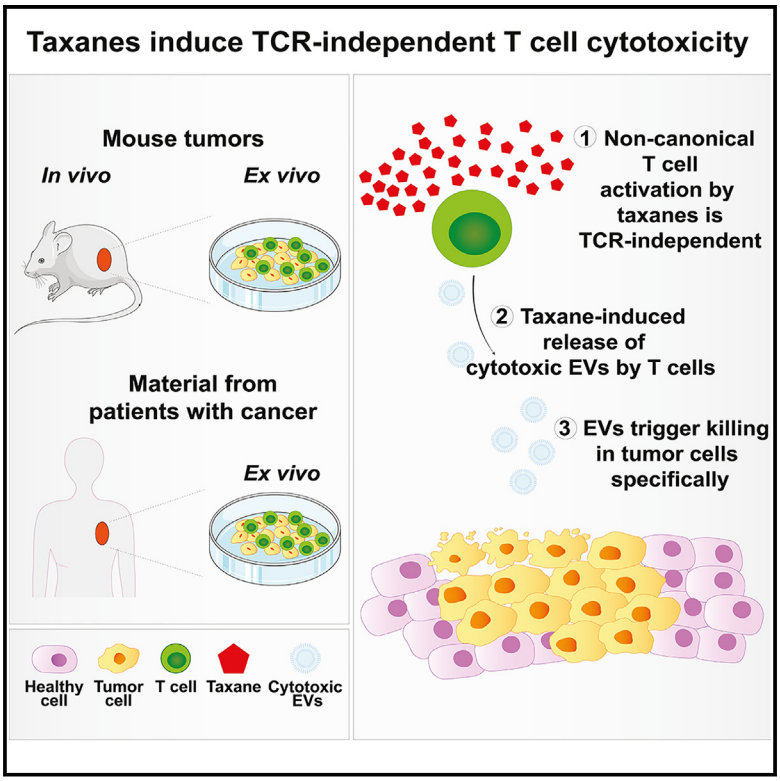

Highlights

- T cells mediate taxane cytotoxicity *in vivo*
- Taxanes trigger T cells to release cytotoxic extracellular vesicles
- Taxanes increase TCR-independent and TCR-mediated T cell killing
- T cells treated *ex vivo* with taxanes can eradicate tumors *in vivo*

Authors

Claire Vennin, Chiara M. Cattaneo, Leontien Bosch, ..., Dirk M. Pegtel, Emile E. Voest, Jacco van Rheenen

Correspondence

j.v.rheenen@nki.nl

In brief

Discrepancies exist between the *in vitro* versus *in vivo* mode of action of taxanes. Vennin et al. uncover that taxanes directly trigger T cells to kill tumor cells by inducing a release of cytotoxic extracellular vesicles. This cytotoxic activity has strong therapeutic activity in organoids from patients with cancer and in tumor-bearing mice.

Vennin et al., 2023, Cancer Cell *41*, 1170–1185
June 12, 2023
https://doi.org/10.1016/j.ccell.2023.05.009

CellPress

CellPress
OPEN ACCESS

Cancer Cell

Article

Taxanes trigger cancer cell killing *in vivo* by inducing non-canonical T cell cytotoxicity

Claire Vennin,[1,2] Chiara M. Cattaneo,[2,3] Leontien Bosch,[4] Serena Vegna,[2,5] Xuhui Ma,[2,3] Hugo G.J. Damstra,[6] Moreno Martinovic,[7] Efi Tsouri,[2,5] Mila Ilic,[2,8] Leyla Azarang,[9] Jan R.T. van Weering,[10] Emilia Pulver,[1,2] Amber L. Zeeman,[2,11,12] Tim Schelfhorst,[1,2] Jeroen O. Lohuis,[1,2] Anne C. Rios,[2,12] Johanna F. Dekkers,[2,12] Leila Akkari,[2,5] Renee Menezes,[9] Rene Medema,[2,8] Serena R. Baglio,[13] Anna Akhmanova,[6] Sabine C. Linn,[14,15] Simone Lemeer,[16,17] Dirk M. Pegtel,[4] Emile E. Voest,[2,3] and Jacco van Rheenen[1,2,18,*]

[1]Division of Molecular Pathology, the Netherlands Cancer Institute, Antoni van Leeuwenhoek Hospital, 1066CX Amsterdam, the Netherlands
[2]Oncode Institute, Amsterdam, the Netherlands
[3]Department of Molecular Oncology and Immunology, the Netherlands Cancer Institute, Antoni van Leeuwenhoek Hospital, 1066CX Amsterdam, the Netherlands
[4]Department of Pathology, Amsterdam UMC, Vrije Universiteit Amsterdam, 1081HV Amsterdam, the Netherlands
[5]Division of Tumor Biology and Immunology, Oncode Institute, the Netherlands Cancer Institute, 1066CX Amsterdam, the Netherlands
[6]Cell Biology, Neurobiology and Biophysics, Department of Biology, Faculty of Science, Utrecht University, 3584CT Utrecht, the Netherlands
[7]Division of Gene Regulation, the Netherlands Cancer Institute, Antoni van Leeuwenhoek Hospital, 1066CX Amsterdam, the Netherlands
[8]Division of Cell Biology, the Netherlands Cancer Institute, Antoni van Leeuwenhoek Hospital, 1066CX Amsterdam, the Netherlands
[9]Biostatistics Centre & Department of Psychosocial Research and Epidemiology, the Netherlands Cancer Institute, 1066CX Amsterdam, the Netherlands
[10]Department of Human Genetics, Center for Neurogenomics and Cognitive Research, Amsterdam UMC, 1105AZ Amsterdam, the Netherlands
[11]Hubrecht Institute, Royal Netherlands Academy of Arts and Sciences (KNAW) and University Medical Centre (UMC), 3584CT Utrecht, the Netherlands
[12]Princess Maxima Center for Pediatric Oncology, 3584CT Utrecht, the Netherlands
[13]Department of Pathology, Cancer Center Amsterdam, Amsterdam University Medical Center, Amsterdam, the Netherlands
[14]Divisions of Molecular Pathology and of Medical Oncology, the Netherlands Cancer Institute, 1066CX Amsterdam, the Netherlands
[15]Department of Pathology, University Medical Center, 1081HV Utrecht, the Netherlands
[16]Biomolecular Mass Spectrometry and Proteomics, Bijvoet Center for Biomolecular Research and Utrecht Institute for Pharmaceutical Sciences, Utrecht University, 3584CT Utrecht, the Netherlands
[17]Netherlands Proteomics Center, 3584CT Utrecht, the Netherlands
[18]Lead contact
*Correspondence: j.v.rheenen@nki.nl
https://doi.org/10.1016/j.ccell.2023.05.009

SUMMARY

Although treatment with taxanes does not always lead to clinical benefit, all patients are at risk of their detrimental side effects such as peripheral neuropathy. Understanding the *in vivo* mode of action of taxanes can help design improved treatment regimens. Here, we demonstrate that *in vivo*, taxanes directly trigger T cells to selectively kill cancer cells in a non-canonical, T cell receptor-independent manner. Mechanistically, taxanes induce T cells to release cytotoxic extracellular vesicles, which lead to apoptosis specifically in tumor cells while leaving healthy epithelial cells intact. We exploit these findings to develop an effective therapeutic approach, based on transfer of T cells pre-treated with taxanes *ex vivo*, thereby avoiding toxicity of systemic treatment. Our study reveals a different *in vivo* mode of action of one of the most commonly used chemotherapies, and opens avenues to harness T cell-dependent anti-tumor effects of taxanes while avoiding systemic toxicity.

INTRODUCTION

Taxanes are among the most widely employed chemotherapies for the treatment of cancer[1] but have also detrimental toxic side effects, some of which irreversible, such as peripheral neuropathy, febrile neutropenia, seizure, and encephalopathy. Although all patients treated with taxanes are exposed to these adverse side effects, not all patients experience clinical benefit. For example, a meta-analysis of long-term outcomes of 100,000 patients with breast cancer revealed that the addition of taxanes to anthracycline regimens prolongs survival in only ~3% of patients.[2] In order to maximize the anti-tumor effects of taxanes while limiting their toxicity, understanding the *in vivo* mode of action of taxanes is critical, however this remains controversial. For

over four decades, the anti-cancer activity of taxanes, such as docetaxel and paclitaxel, has mainly been attributed to their ability to trigger abnormal mitotic spindle formation by stabilizing microtubules, leading to delayed mitotic progression and ultimately cell death, based mostly on *in vitro* studies.[3] Conversely, data from both animal models and in patients with cancer suggest that taxanes may induce apoptosis independent of blocking mitotic progression in the *in vivo* setting.[4–6] For instance, we previously reported that taxanes trigger apoptosis in cancer cells *via* perturbing mitosis progression *in vitro*, while taxane-mediated killing of the same cancer cells growing in an *in vivo* environment was independent of such mitotic defects.[5] Similarly, analysis of human and mouse tumor tissues showed that treatment with taxanes induces only a moderate increase in mitotic index, which does not correlate with tumor response to treatment.[6–9] Together, these studies indicate that alternative, mitotic-independent mechanisms of action of taxanes must be active *in vivo*; however such mechanisms have yet to be uncovered.

One major difference between the *in vitro* and *in vivo* experimental settings is the presence of immune cells in the microenvironment, even in immunocompromised models of cancer where some immune functions and immature immune cells are maintained. This may be particularly relevant for taxane treatments since chemotherapies can influence immune reactions in the context of cancer.[10–15] As such, in addition to killing cancer cells, chemotherapy can influence immune responses *via*, for instance, inducing immunogenic cell death (ICD) and chromosome instability or modifying epitope presentation by cancer cells.[16–18] Considering that the tumor microenvironment (TME) can be highly heterogeneous among patients, a role of the TME in driving the anti-tumor effects of taxanes may explain the partial response to taxanes in the clinic. Modulations of the tumor immune microenvironment upon taxanes have been reported in a handful of studies.[18–20] For instance, we recently reported that patients with breast cancer with a high tumor lymphocyte infiltration have a better clinical response to taxane-containing chemotherapy compared to a chemotherapy regimen that does not include taxanes.[19] Although these studies point to a potential role of the immune microenvironment in driving the *in vivo* anti-tumor effects of taxanes, the molecular mechanisms underlying such action of taxane-induced cell death are still unknown.

In this study, we aim to characterize the mode of action of taxane-mediated killing in the *in vivo* setting. Using mouse and patient-derived models of cancer, autologous organoid and T cell co-culture platforms and proteomic analyses, we uncover that taxanes can directly activate T cells to specifically eradicate tumor cells. Mechanistically, we demonstrate that taxanes induce a release of cytotoxic extracellular vesicles by T cells that subsequently trigger tumor death. We also reveal that T cells pre-treated with taxanes *ex vivo* have an anti-tumor capacity once transplanted *in vivo*. These findings establish a mode of action of taxanes *in vivo*, one of the most widely used chemotherapies for cancer treatment. Critically, our study provides a therapeutic approach to exploit an optimal T cell-dependent anti-tumor activity of taxanes while avoiding systemic exposure to their toxicity.

RESULTS

T cells promote the *in vivo* anti-tumor effects of taxanes

Considering that taxane-induced cell death is classically thought to be mediated by impairing mitotic progression,[3,21,22] we first tested whether this mechanism held true *in vivo* in two immunocompetent mouse models of breast cancer that are based on the loss of tumor suppressor genes *Brca1* and *Trp53* (KB1P model[23]) or on the overexpression of the oncogene *PyMT* (MMTV-PyMT model[24]). Docetaxel treatment in mice bearing tumors delayed tumor outgrowth, confirming that these tumor models were sensitive to docetaxel (Figures S1A–S1C). However, we did not observe a significant accumulation of mitotic figures in tumors isolated 24h after the second docetaxel administration (Figures S1D and S1E), which would be expected if the anti-tumor effects of docetaxel occurred mostly through perturbation of mitosis. This suggested that killing of cancer cells upon docetaxel in KB1P and MMTV-PyMT tumors was not mediated by delayed mitotic progression *in vivo* alone and is in line with previous reports in other animal cancer models and samples from patients with cancer.[5,7–9,19]

This prompted us to investigate the differing mode of action of docetaxel in the *in vivo* setting. We previously reported in the MATADOR trial cohort patients with estrogen receptor (ER)/progesterone receptor (PR) positive or triple-negative breast cancer that differential survival upon docetaxel-containing chemotherapies correlate with the presence of specific populations of immune cells within tumors.[19] In particular, we observed that adding docetaxel (T) to the doxorubicin + cyclophosphamide (AC) chemotherapy regimen provided a survival benefit only to patients with high tumor-infiltrating lymphocytes (TILs) content.[19] Therefore, we interrogated the biological relevance of this correlation in mouse models of breast cancer. Friend Virus B (FVB) mice carrying KB1P tumors were subjected to treatment with an IgG control or with depleting antibodies against $CD4^+$ and $CD8^+$ expressing cells, as previously achieved,[25] prior to treatment with either AC or AC + T (Figure 1A). The reduction of intratumoral T cells upon treatment with depleting antibodies was confirmed by immunohistochemistry (Figures S1F and S1G). In patients with breast cancer, AC treatment leads to a 5-year overall survival of ~90%, which is moderately improved (~3%) upon taxane (T) addition.[2] Similar to these clinical observations, treating mice bearing tumors with AC led to a large reduction in tumor volume in both the IgG control mice and the T cell-depleted mice, showing the high anti-tumor activity of AC (Figure 1B and Data S1) and in line with previous work demonstrating that T cells do not influence tumor response to non-taxane chemotherapies.[26] However, small tumors persisted during the course of the treatment with AC (dotted line in Figure 1B). Importantly, the addition of docetaxel to AC triggered a complete response with no detectable tumors during the course of the treatment in the IgG control but not in the T cell-depleted mice (Figure 1C and Data S1), suggesting that T cells support the docetaxel-mediated complete reponse. These data align with the correlation between high intratumoral T cell levels and improved response to taxane-containing chemotherapy reported in patients with breast cancer.[19]

To further test whether T cells mediated the anti-tumor activity of docetaxel, we used fluorescence-activated cell sorting (FACS)

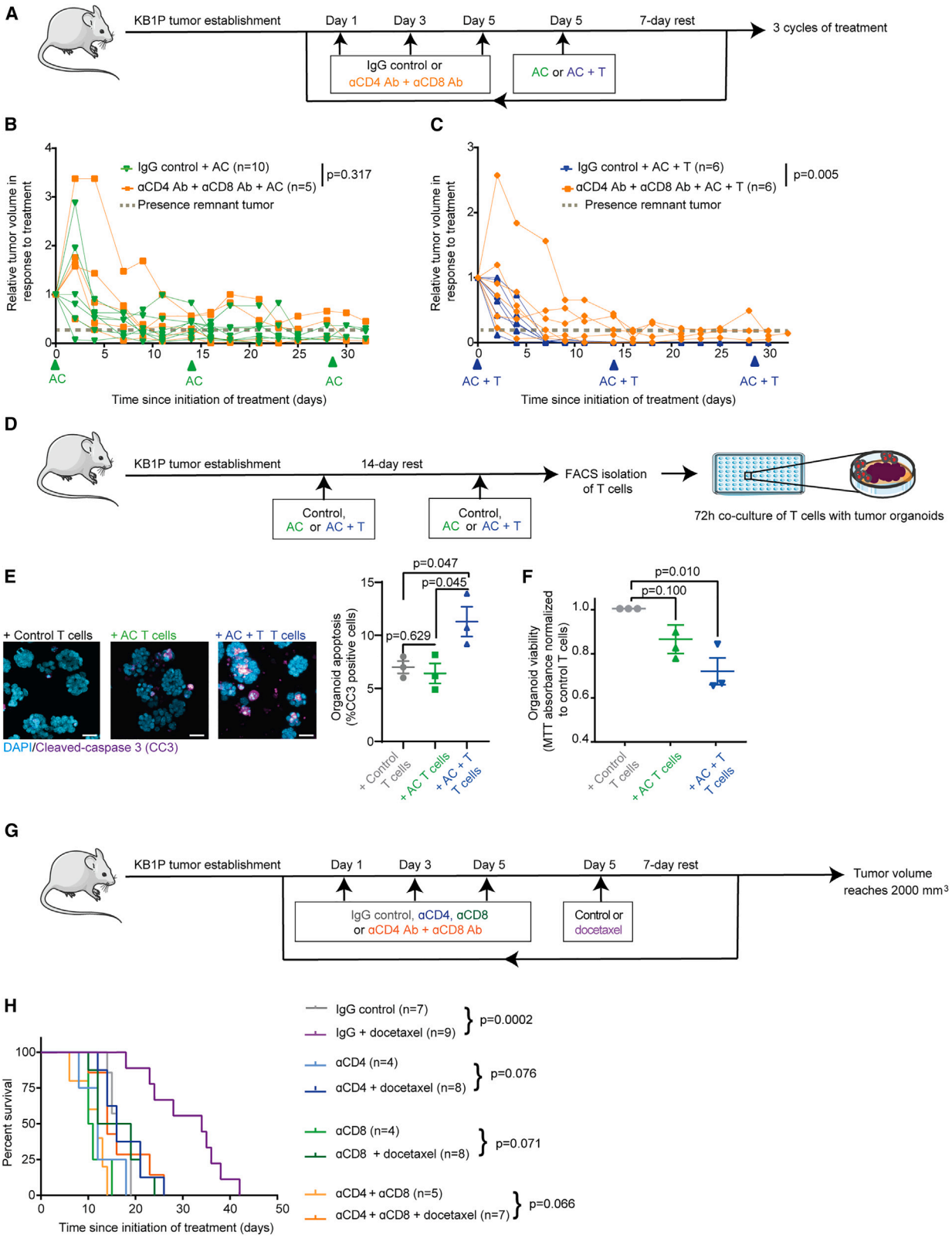

(legend on next page)

to isolate T cells from KB1P mammary tumors grown in mice that had been treated with two cycles of either control, AC or AC + T (Figures 1D and S1H). FACS quantification revealed an increased infiltration of T cells into tumors treated with AC + T compared to control or AC treatments (Figure S1I). Subsequently, the cytotoxic capacity of the isolated intratumoral T cells was tested by co-culturing them with matched KB1P tumor-derived organoids (Figure 1D). Co-cultures with AC + T-treated intratumoral T cells led to an increase in organoid apoptosis and a reduction in the number of surviving organoids compared to the co-cultures with control or AC-treated intratumoral T cells (Figures 1E and 1F). Next, we tested whether these observations also held true for MMTV-PyMT tumors. Similar to KB1P tumors, we observed a higher infiltration of T cells upon AC + T treatment compared to control and AC treatments (Figure S1J). Additionally, co-cultures of organoids with T cells isolated from AC + T-treated tumors led to reduced organoid viability in comparison to their co-culture counterparts with T cells isolated from control or AC-treated MMTV-PyMT tumors (Figure S1K).

We next investigated the individual roles of $CD4^+$ *versus* $CD8^+$ T cells in driving tumor response to docetaxel (Figure 1G). In line with the increased intratumoral T cell infiltration upon treatment with AC + T compared to AC (Figure S1I), docetaxel treatment correlated with enhanced $CD4^+$ and $CD8^+$ T cell infiltration in KB1P tumors (Figures S1I and S1M). In addition, depletion of either $CD4^+$ T cells alone, $CD8^+$ T cells alone or both $CD4^+$ and $CD8^+$ T cells abrogated the anti-tumor effects of docetaxel treatment in both KB1P and MMTV-PyMT tumors (Figures 1H and S1N). This demonstrated that both $CD4^+$ and $CD8^+$ T cell populations contribute to tumor response to docetaxel treatment.

Docetaxel does not sensitize cancer cells to T cell-mediated killing

We next investigated how docetaxel triggered the observed enhanced cytotoxic capacity of T cells. We initially hypothesized that docetaxel might alter the immune properties of tumor cells. However, considering that untreated tumor organoids were more efficiently killed by T cells isolated from tumors treated with AC + T compared to AC alone (Figures 1E and 1F), the enhanced T cell cytotoxicity might not be caused by modulation of the immune properties of the cancer cell compartment. To confirm this, we tested the ability of T cells isolated from control KB1P tumors to kill KB1P organoids that were pre-treated with low, non-lethal doses of AC or AC + T (Figure S2A). After 72h of pre-treating the organoids, we renewed the culture media and washed the drugs away prior to co-culturing these organoids with T cells isolated from control-treated KB1P tumors (Figure S2A). We found that the addition of docetaxel during pre-treatment of the organoids (AC + T) did not alter the number of living organoids upon co-culture with the control T cells (Figure S2B). This confirmed that a potential change in the immune properties of tumor cells does not contribute largely to the anti-tumor activity of docetaxel that we observed in Figures 1E and 1F. Instead, the anti-tumor activity of docetaxel may be mediated by other contributors, such as the properties of the T cells themselves.

Docetaxel directly increases T cell cytotoxic activity

We then assessed whether docetaxel might instead directly influence the killing ability of T cells. To test this, $CD4^+$ and $CD8^+$ T cells were separately isolated by FACS from the spleens of non-tumor-bearing, drug naïve FVB female mice (Figures 2A and S2C). Following isolation, splenic T cells were treated *in vitro* for 72h with 10 nmol/L of docetaxel, a dose that did not induce significant killing of T cells (Figure S2D) but that increased microtubule density, in line with the known microtubule-stabilizing effect of taxanes (Figures S2E and S2F)[21,22] and that is relevant to the dose used *in vivo*.[27] We next co-cultured these T cells with drug-naïve KB1P organoids (Figure 2A). Intriguingly, we observed an increased apoptotic rate and a reduction of living organoids when co-cultured with either $CD4^+$ or $CD8^+$ T cells pre-treated with docetaxel compared to their control counterparts (Figures 2B and 2C). To confirm the taxane-specific induction of T cell-killing capacity, splenic T cells were treated with a low dose of paclitaxel (another taxane, Figure S2G) or carboplatin (a non-taxane chemotherapy, Figure S2H) prior to co-culturing them with tumor-derived organoids. Similar to our previous observations, paclitaxel-treated T cells triggered a decrease in tumor organoid survival compared to control T cells, whereas carboplatin-treated T cells did not

Figure 1. T cells mediate the *in vivo* anti-tumor effects of docetaxel

(A) Schematic representation of experimental design and treatment timeline in the KB1P tumor model.

(B and C) KB1P tumor volume over the course of treatment with doxorubicin + cyclophosphamide (AC) (B) or with AC + docetaxel (T) (C) in the presence (IgG control) or absence of T cells (αCD4 Ab + αCD8 Ab) and normalized to the initial tumor volume when the treatment is initiated. Dotted gray line indicates the threshold of tumor detection. p-values for 1B and 1C were obtained from the raw values corresponding to the data depicted in 1B and 1C and that were analyzed in R using a linear mixed-effects model.

(D) Schematic representation of experimental design for isolation of intratumoral T cells followed by co-culture with organoids. Following *in vivo* treatment with a vehicle control, AC or AC + T, KB1P tumors were excised and intratumoral $CD4^+$ and $CD8^+$ T cells were isolated by Fluorescence-Activated Cell Sorting (FACS) and co-cultured with chemotherapy-naïve KB1P organoids.

(E) Representative images and quantification of immunofluorescence staining for cleaved-caspase 3 (CC3) in KB1P organoids following co-culture with $CD4^+$ and $CD8^+$ T cells isolated from KB1P tumors treated with a vehicle control, AC or AC + T. Scale bar = 50 μm. n = 3 biological repeats. Data are presented as mean ± standard-error of the mean (SEM).

(F) MTT assay assessment of KB1P organoid survival following co-culture with $CD4^+$ and $CD8^+$ T cells isolated from KB1P tumors treated with a vehicle control, AC or AC + T. n = 3 biological repeats with three technical replicates *per* repeat. Data are presented as mean with SEM. For E and F, p values were determined using unpaired, nonparametric t-test with a Mann-Whitney U correction in GraphPad Prism. Data are presented as mean ± SEM.

(G) Schematic representation of experimental design and treatment timeline.

(H) Kaplan-Meier survival curve for mice bearing KB1P tumors treated with a vehicle control or docetaxel upon administration of an IgG control (gray and purple lines) or of depleting antibodies against $CD4^+$ T cells only (blue lines), $CD8^+$ T cells only (green lines) or $CD4^+$ and $CD8^+$ T cells (orange lines). p values were determined using a log rank Mantel-Cox test in GraphPad Prism. See also Figures S1 and S2, as well as Data S1.

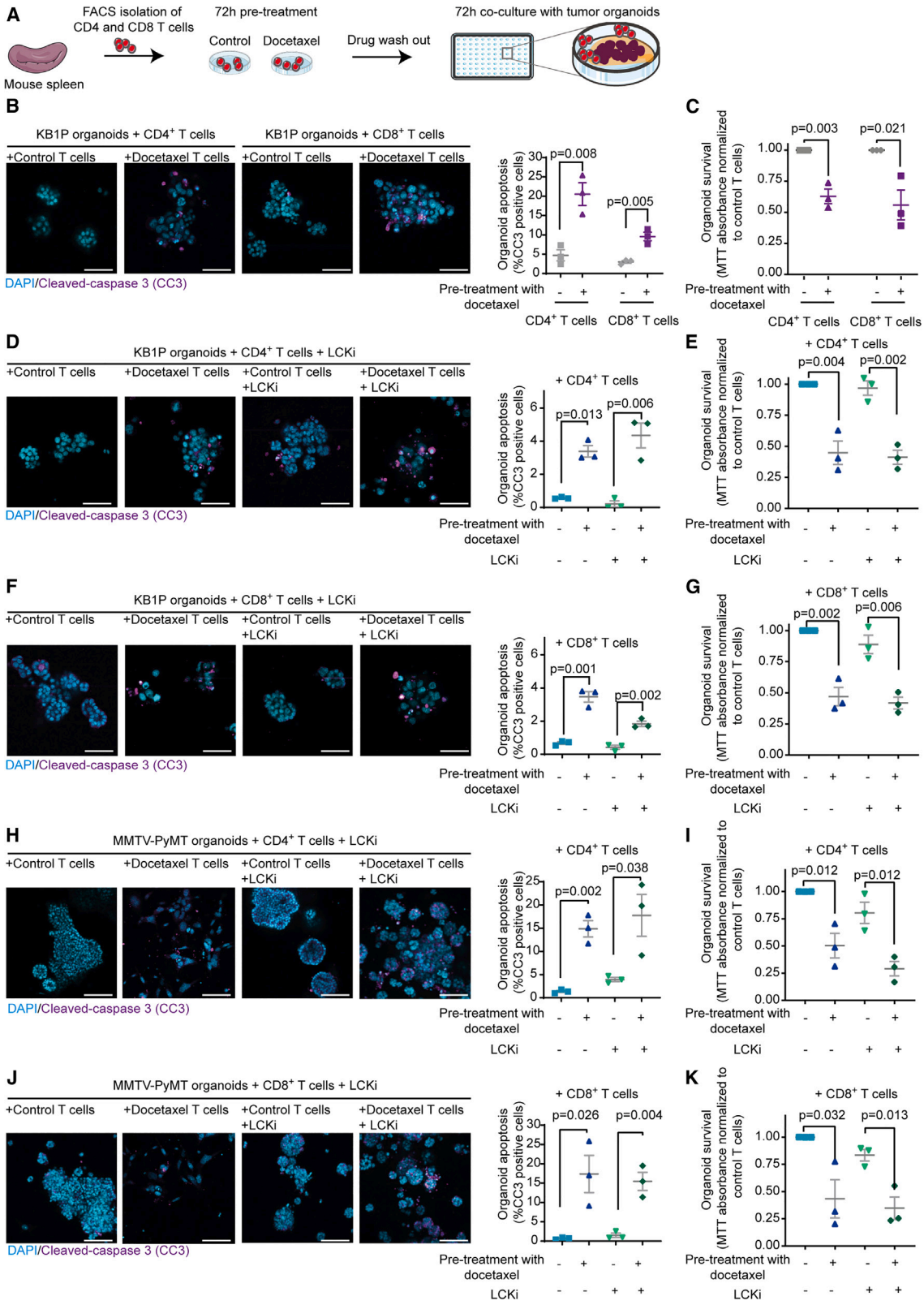

(legend on next page)

(Figures S2I–S2L), thereby confirming the taxane-specificity of our observations in both models.

Docetaxel-induced T cells killing is independent of TCR activation

Classical T cell-mediated killing requires specific recognition of an antigen presented by MHC molecules on the target cell by the T cell receptor (TCR).[28] However, because we isolated T cells from spleens of tumor-naïve mice, which were co-cultured with tumor organoids for only a short duration, this specific tumor organoid-T cell interaction was lacking in our setup (Figure 2A). Moreover, treatment with docetaxel did not lead to significant alterations in the expression levels of markers of canonical T cell activation or in the secretion of cytokines that are known to be released upon canonical T cell activation (Figures S2M and S2N). Therefore, we hypothesized that elimination of tumor organoids by T cells pre-treated with docetaxel was independent of a specific TCR-antigen recognition. To test this, we isolated splenic T cells from Rosa26^{mTmG} FVB mice and employed live microscopy to visualize their interactions with KB1P organoids over time *in vitro*. In line with our T cell-mediated killing assay (Figures 2B and 2C), we observed over time a reduction of KB1P organoids growth when co-cultured with either CD4$^+$ or CD8$^+$ T cells pre-treated with docetaxel (Figures S3A and S3B). The killing of cancer organoids was not accompanied by a large infiltration of T cells into the center of the basement membrane extract (BME) to reach the organoids (Figures S3C and S3D). This demonstrated that T cell-mediated killing upon docetaxel treatment did not require physical contact between a T cell and a cancer cell. To confirm this, we assessed whether inhibition of TCR signaling with a potent and selective inhibitor of lymphocyte cell kinase (LCKi)[29] would influence the T cell-killing capacity upon docetaxel treatment. LCK inhibition reduced killing of MMTV-PyMT organoids expressing OVA by T cells isolated from inbred OT I mice,[30,31] confirming the ability of the LCK inhibitor to block TCR-mediated killing (Figure S3E). Importantly, LCK inhibition did not impair the ability of docetaxel to increase the cytotoxic activity of either CD4$^+$ or CD8$^+$ tumor naive T cells against KB1P organoids (Figures 2D–2G). The direct and TCR-independent increase of T cell-mediated killing upon docetaxel treatment was also confirmed in MMTV-PyMT organoids (Figures 2H–2K). Lastly, to genetically confirm our findings, we isolated T cells from the spleen of NOD-SCID *Il2rg*$^{-/-}$ mice, which cannot mature nor produce a TCR response. Pre-treatment with docetaxel triggered T cell-mediated killing of KB1P organoids in this setting (Figure S3F), further confirming the TCR-independent killing by docetaxel-treated T cells.

Considering that T cell killing upon docetaxel does not appear to rely on TCR activation, we tested whether docetaxel-treated T cells also kill healthy epithelial organoids. We co-cultured docetaxel-treated T cells with healthy mouse mammary epithelial cells (MECs) grown in 3D BME. Intriguingly, we found that apoptosis was induced in only a minor fraction of MECs that were co-cultured with either CD4$^+$ or CD8$^+$ T cells pre-treated with docetaxel, in contrast to the high levels of apoptosis in cancer organoids (Figure S3G). Additionally, MEC survival was less reduced when co-cultured with docetaxel-treated CD4$^+$ or CD8$^+$ T cells compared to the tumor organoids (Figure S3H). Together, our data provide evidence that docetaxel treatment induces a TCR-independent T cell killing of cancer organoids specifically, without triggering apoptosis in healthy organoids.

Docetaxel increases the anti-tumor activity of human T cells

We next seeked to test the relevance of our findings in the human setting. We worked with Jurkat T cells, an immortalized line of human T lymphocyte cells that is frequently used to study T cell signaling.[32] Importantly, the Jurkat T cells were not engineered to specifically recognize target cells. Jurkat T cells were pre-treated with 5 nmol/L of docetaxel, a dose that did not significantly reduce the survival of Jurkat T cells (Figure S3I). We co-cultured control- and docetaxel-treated T cells with 7 organoid lines derived from patients with breast cancer and one healthy epithelial mammary organoids (Figure S3J).[33,34] Analysis of cleaved-caspase 3 immunofluorescence staining revealed that in 5 out of the 7 patient-derived organoid lines tested, docetaxel-treated Jurkat T cells significantly enhanced cancer organoid apoptosis compared to control Jurkat T cells (Figures S3K and S3L). We did not observe a significant induction of apoptosis in healthy organoids co-cultured with docetaxel-treated Jurkat T cells (Figures S3M and S3N). Next, we tested the ability of docetaxel to induce Jurkat T cell-mediated killing in cancer cell lines derived from human breast tumor, lung adenocarcinoma, melanoma, glioma, cholangiocarcinoma, hepatocellular

Figure 2. Docetaxel directly increases T cell cytotoxic activity

(A) Schematic representation of the isolation of splenic T cells and co-culture with tumor organoids.

(B) Representative images and quantification of immunofluorescent staining for cleaved-caspase 3 (CC3) in KB1P organoids following co-culture with either CD4$^+$ or CD8$^+$ T cells pre-treated with a vehicle control or with docetaxel. Scale bar = 100 μm.

(C) MTT assay assessment of KB1P organoid survival following co-culture with CD4$^+$ or CD8$^+$ T cells, pre-treated with a vehicle control or with docetaxel.

(D and E) Representative images and quantification of immunofluorescent cleaved-caspase 3 staining in KB1P organoids and E. MTT assay assessment of KB1P organoid survival, following co-culture with CD4$^+$ T cells pre-treated with a vehicle control or with docetaxel, in the presence or absence of an LCK inhibitor (LCKi). Scale bar = 100 μm.

(F and G) Representative images and quantification of immunofluorescent cleaved-caspase 3 staining in KB1P organoids and G. MTT assay assessment of KB1P organoid survival, following co-culture with CD8$^+$ T cells pre-treated with a vehicle control or with docetaxel, in the presence or absence of an LCKi. Scale bar = 100 μm.

(H and I) Representative images and quantification of immunofluorescent cleaved-caspase 3 staining (H) and MTT assay assessment of organoid survival (I) in MMTV-PyMT organoids following co-culture with CD4$^+$ T cells pre-treated with a vehicle control or with docetaxel, in the presence or absence of an LCKi. Scale bar = 100 μm.

(J. and K) Representative images and quantification of immunofluorescent cleaved-caspase 3 staining (J) and MTT assay assessment of organoid survival (K) in MMTV-PyMT organoids following co-culture with CD8$^+$ T cells pre-treated with a vehicle control or with docetaxel, in the presence or absence of an LCKi. Scale bar = 100 μm. n = 3 biological repeats with three technical replicates *per* repeat. For Figure 2, p values were determined using unpaired, nonparametric t-test with a Mann-Whitney U correction in GraphPad Prism. Data are presented as mean ± SEM. See also Figures S2–S4.

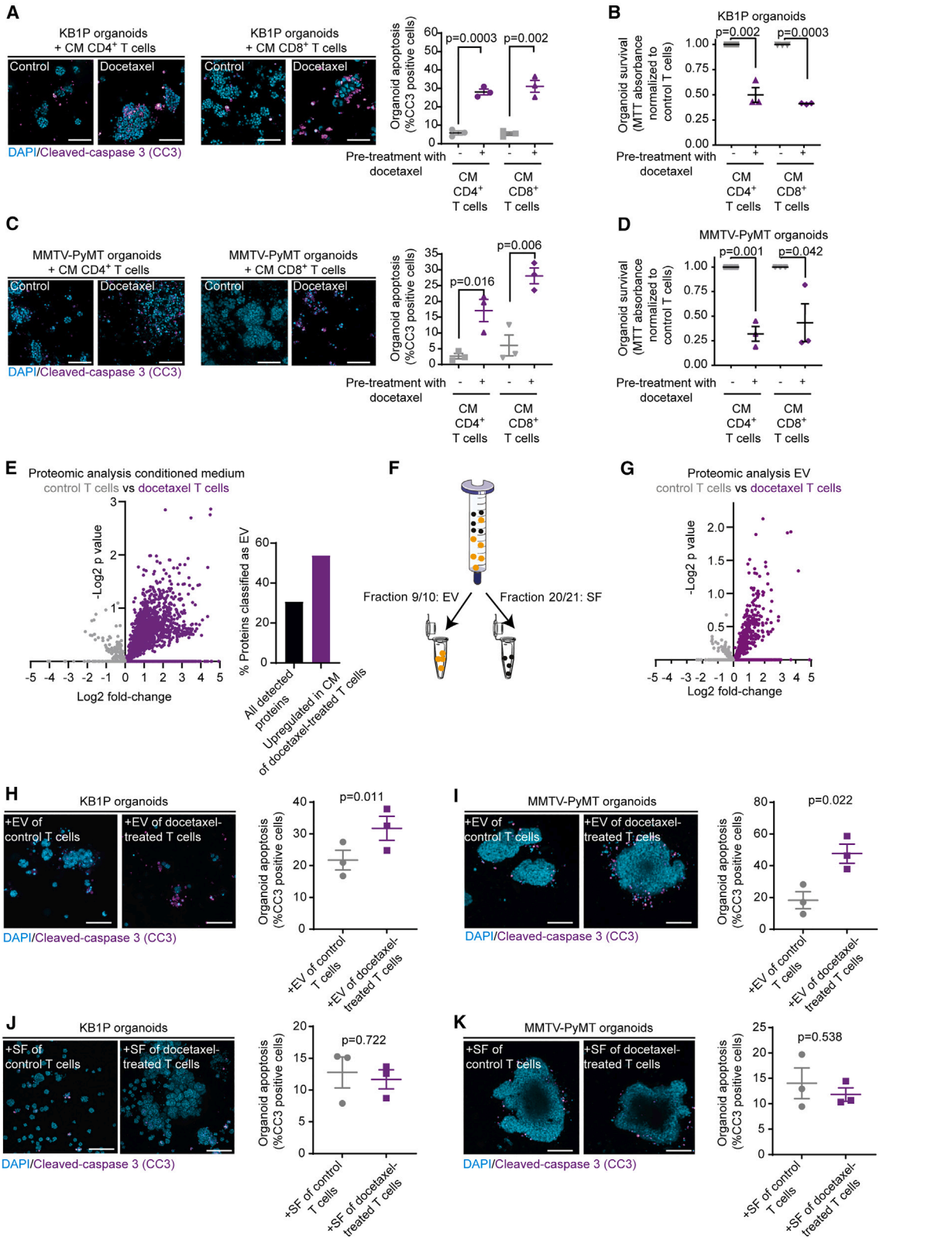

(legend on next page)

carcinoma or rectal carcinoma (Figures S4A–S4H), as well as in human healthy retinal pigment epithelium (RPE) cells and human embryonic kidney 293 (HEK293T) cells (Figures S4I and S4J). In this context, we found that in six out of eight human cancer cell lines and none of the human healthy cell lines studied, Jurkat T cells pre-treated with docetaxel increased apoptosis compared to control Jurkat T cells (Figure S4). However, compared to the 3D tumor organoid setting (Figures S3I–S3N), the induction of apoptosis in these 2D cancer cell lines co-cultured with docetaxel-treated Jurkat T cells seemed more moderate. Combined, these results demonstrate that docetaxel induces T cell cytotoxicity against tumor cells specifically, not only in the murine setting but also in the context of human cancer models.

Docetaxel triggers T cells to release non-classical cytotoxic factors

Our data demonstrated that T cell-mediated killing upon docetaxel did not require a direct contact between T cells and tumor organoids (Figures S3C and S3D) and was not mediated by the TCR (Figures 2D–2K) nor by classical T cell activation (Figures S2M and S2N). This prompted us to assess whether docetaxel triggered T cells to release non-classical cytotoxic factors, which in turn eliminated tumor organoids. We first tested the response of KB1P and MMTV-PyMT organoids to treatment with conditioned media (CM) generated by T cells pre-treated with control or docetaxel. We found that both cancer organoid lines had an increased organoid apoptosis and a reduced live organoid count when treated with CM derived from either $CD4^+$ or $CD8^+$ T cells that were pre-treated with docetaxel compared to the control T cell (Figures 3A–3D). We measured the sensitivity of KB1P and MMTV-PyMT cancer organoids to docetaxel and found that the IC_{50} of both lines ($IC_{50(KB1P)}$ = 90.49 nmol/L and $IC_{50(MMTV\text{-}PyMT)}$ = 130.1 nmol/L) was much higher than the concentration of docetaxel present in CM (10 nmol/L before diluted with organoid medium 1:1) (Figures S5A and S5B). This confirmed that the induction of organoid apoptosis and the reduced cancer organoid survival upon CM treatment were mostly caused by factors released by T cells upon docetaxel treatment rather than by docetaxel that was still present in the CM. Moreover, to test whether taxane is stored by T cells during treatment and released to target cells, we co-cultured paclitaxel-treated Jurkat T cells with HeLa cells that overexpressed ABCB1 (Pgp). Pgp is an ABC transporter that drives the efflux of compounds such as paclitaxel,[35] and thereby provides resistance to this drug (Figure S5C). Paclitaxel-treated Jurkat T cells induced apoptosis and reduced survival in Hela ABCB1 cells to a similar level as for HeLa WT cells (Figures S5D and S5E). It is therefore unlikely that cancer cell killing by taxane-treated T cells is caused by an uptake and release of taxanes by T cells.

Docetaxel induces a release of cytotoxic extracellular vesicles by T cells to eliminate tumor organoids

In order to identify the secreted factors that may be potentially responsible for killing tumor organoids, we next used mass spectrometry to profile the secretome of $CD4^+$ and $CD8^+$ T cells treated with docetaxel. Because fetal bovine serum (FBS) used in culturing media contains many proteins that could interfere with mass spectrometry analysis, we first confirmed that T cells pre-treated with docetaxel in the absence of FBS could also target KB1P and MMTV-PyMT organoids (Figures S5F and S5G). We grouped $CD4^+$ and $CD8^+$ T cells together in order to obtain enough secreted protein for analysis. Intriguingly, the protein content in the CM from docetaxel-treated T cells was much higher compared to that from control T cells CM (Figure 3E and Table S1). We did not find significant differences in factors that have been reported to drive canonical T cell-mediated killing (Table S1). Instead, Gene ontology annotation (http://geneontology.org) revealed that proteins that are known to be the cargos of extracellular vesicles (EVs) were over-represented in the CM from docetaxel-treated T cells (Figure 3E, bar graph and Table S1, see proteins in bold). This triggered us to fractionate the CM into an EV fraction and a soluble fraction (SF) (fractions 9/10 and fractions 20/21, respectively) using a generally used size exclusion chromatography protocol (Figure 3F).[36] We isolated the CM and subsequently the EV fraction and soluble fraction from 6 × 10^6 mouse splenic T cells that had been treated with either control or docetaxel. Electron microscopy and NanoSight particle analysis confirmed the presence of EVs in the EV fractions, with a particle diameter of up to 250 nm (Figure S5H). We next performed proteomics analysis of the EV

Figure 3. Docetaxel induces a release of cytotoxic extracellular vesicles by T cells to eliminate tumor organoids

(A and B) Representative images and quantification of immunofluorescent staining for cleaved-caspase 3 (CC3) (A) and MTT assay assessment of organoid survival (B) in KB1P organoids upon treatment with conditioned media generated by $CD4^+$ T cells or $CD8^+$ T cells pre-treated with a vehicle control or with docetaxel.

(C and D) Representative images and quantification of immunofluorescent staining for cleaved-caspase 3 (C) and MTT assay assessment of organoid survival (D) in MMTV-PyMT organoids upon treatment with conditioned media generated by $CD4^+$ or $CD8^+$ T cells pre-treated with a vehicle control or with docetaxel. For A-D, n = 3 biological repeats with three technical replicates *per* repeat, p values were determined using unpaired, nonparametric t-test with a Mann-Whitney U correction in GraphPad Prism and data presented as mean ± SEM.

(E) Volcano plot (left) representing extracellular peptides detected in the secretome of T cells treated with a vehicle control (gray) versus docetaxel (purple) and quantification of percentage of proteins identified as extracellular vesicle (EV) in the conditioned media of docetaxel-treated T cells, compared to all proteins detected in the conditioned media of T cells (right bar graph). n = 3 biological repeats with one technical replicate *per* repeat.

(F) Schematic representation of the isolation of the EV fraction and soluble fraction (SF) released by T cells.

(G) Volcano plot representing the peptides detected in the EV fractions released by control (gray) versus docetaxel-treated (purple) T cells.

(H and I) Representative images and quantification of cleaved-caspase 3 immunofluorescent staining in KB1P organoids (H) and in MMTV-PyMT organoids (I) upon a 72h treatment with EVs isolated from conditioned media generated by control T cells or docetaxel-treated T cells.

(J and K) Representative images and quantification of cleaved-caspase 3 immunofluorescent staining in KB1P organoids (J) and in MMTV-PyMT organoids (K) upon a 72h treatment with the soluble fraction (SF) isolated from conditioned media generated by control T cells or docetaxel-treated T cells. For E, G and H-K, n = 3 biological repeats, data are presented as mean ± SEM, p values were determined using unpaired, nonparametric t-test with a Mann-Whitney U correction in GraphPad Prism. Scale bar = 100 μm. See also Figures S5, Tables S1, and S2.

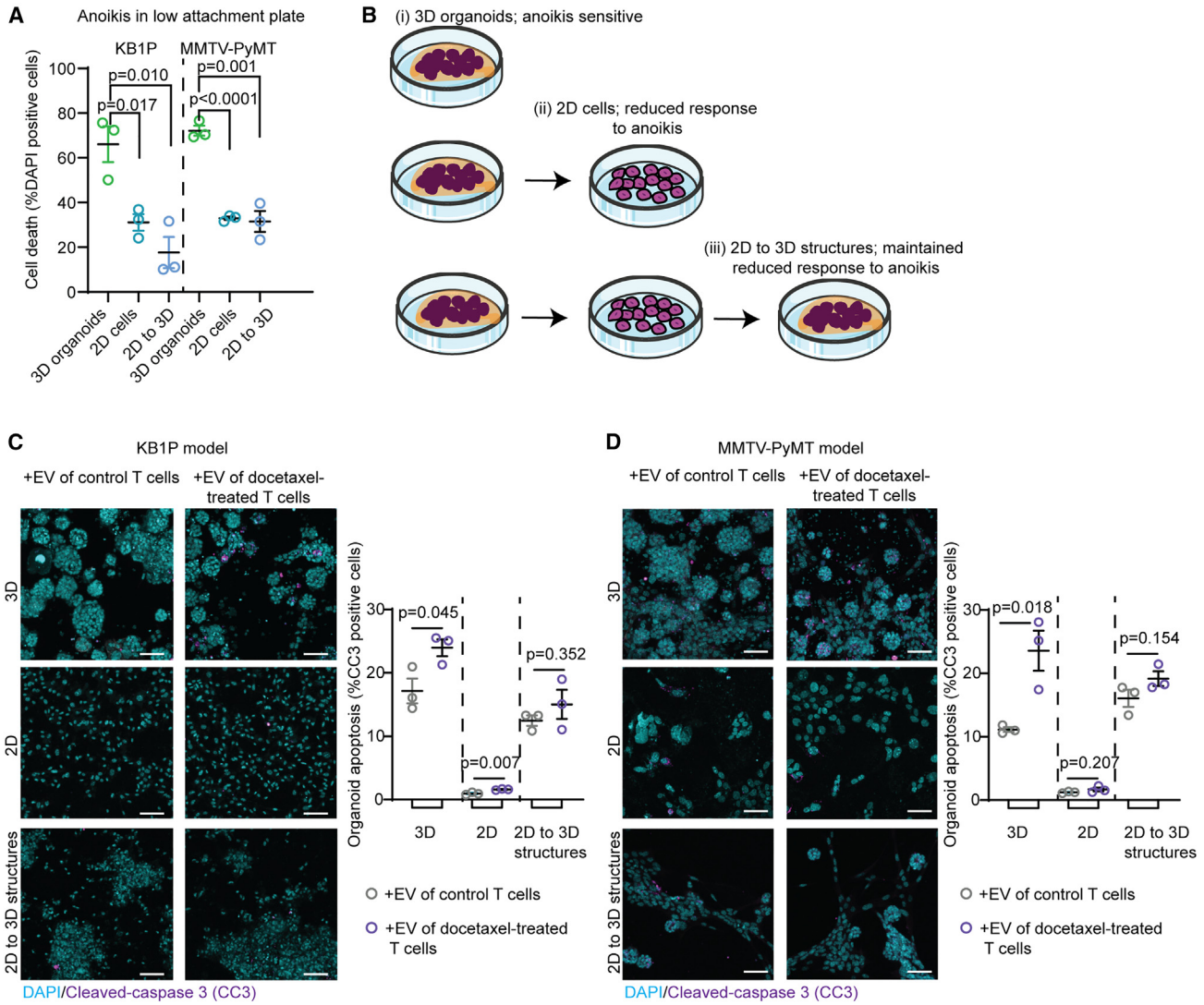

Figure 4. 2D cell lines are less sensitive to EVs released by docetaxel-treated T cells and to anoikis compared to matched 3D organoids

(A) Quantification of cell death in low attachment plate for KB1P and MMTV-PyMT 3D organoids, 2D cells and 2D to 3D organoids. n = 3 biological repeats, data are presented as mean with SEM, p values were determined using unpaired, nonparametric t-test with a Mann-Whitney U correction in GraphPad Prism.

(B) Schematic representation of cultures of matched 3D organoids, 2D cell lines and 2D to 3D organoids.

(C and D) Representative images and quantification of cleaved-caspase 3 immunofluorescence staining in KB1P and (D) MMTV-PyMT 3D organoids, 2D cells, 2D to 3D organoids treated with EVs released by control T cells or docetaxel-treated T cells. n = 3 biological repeats, scale bar = 50 μm. Data are presented as mean ± SEM, p values were determined using unpaired, nonparametric t-test with a Mann-Whitney U correction in GraphPad Prism.

fractions. Approximately 80% of proteins detected in the EV fractions overlapped with those identified in the CM (Figure 3G and Table S2). Importantly, in line with our data in the CM (Figure 3E), we found an increased number of proteins in the EV fraction isolated from docetaxel-treated T cells compared to the EV fraction from the control T cells (Figures 3G and Table S2), which indicates either a differential abundance of EVs or of cargo proteins in EVs upon docetaxel treatment of the T cells. We also attempted to perform transcriptomics analysis of the EV fractions, however the levels of protein coding gene transcripts that we detected were too low to draw meaningful conclusions, likely because of the low amount of RNA contained in the EVs from mouse naïve T cells.

Next, KB1P and MMTV-PyMT organoids were treated with the EV or soluble fractions isolated from 6 × 10^6 T cells. Immunofluorescence analysis of cleaved-caspase 3 demonstrated that the EV fraction isolated from T cells treated with docetaxel-induced apoptosis to a significantly larger extent than the EV fraction isolated from control T cells (Figures 3H and 3I). Moreover, the type and/or the abundance of EVs in the EV fraction isolated from control-treated T cells did not significantly induce apoptosis in tumor organoids compared to treatment with the control PBS (Figure S5I). Importantly, tumor organoids were also treated with the SF isolated from the CM of T cells and that contained secreted soluble factors but no EVs. We did not observe an induction of apoptosis in either organoid lines

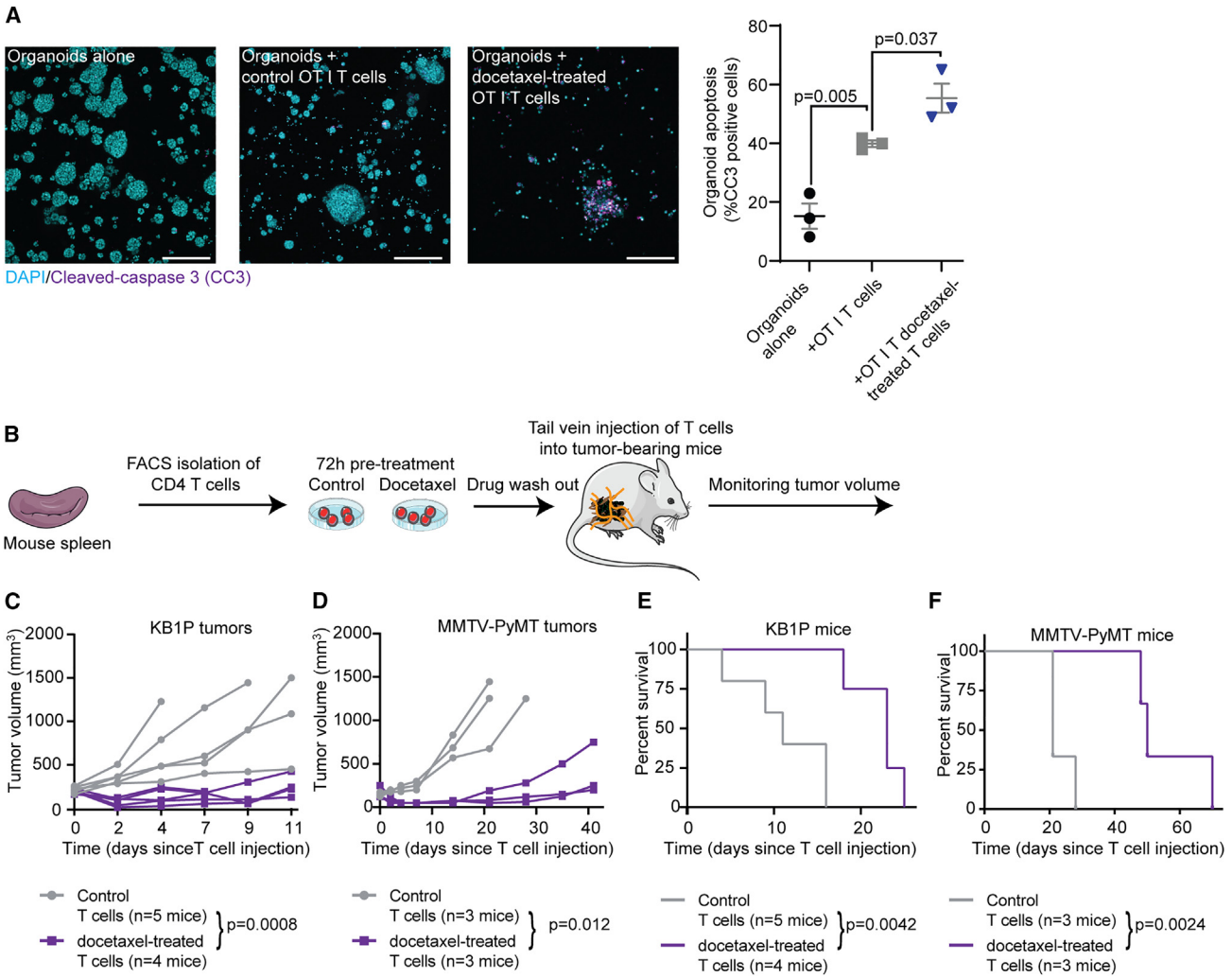

Figure 5. Pre-clinical assessment of the therapeutic benefits of T cells pre-treated with docetaxel

(A) Representative images and quantification of cleaved-caspase 3 (CC3) immunofluorescent staining in MMTV-PyMT organoids expressing OVA and co-cultured with T cells isolated from the spleen of OT I mice upon pre-treatment with a vehicle control or docetaxel. n = 3 biological repeats, scale bar = 100 μm. Data are presented as mean ± SEM, p values were determined using unpaired, nonparametric t-test with a Mann-Whitney U correction in GraphPad Prism.

(B) Schematic representation of experiment design.

(C and D) Tumor growth in mice bearing KB1P tumors (C) or MMTV-PyMT tumors (D) and transplanted with $CD4^+$ T cells pre-treated *in vitro* with a vehicle control or with docetaxel. For Figure 5C, the p value was determined in R using a linear mixed-effects model, for Figure 5D, due to the lower number of animals, the p value was determined in Prism GraphPad using a mixed-effects analysis with a Geisser-Greenhouse correction.

(E and F) Kaplan-Meier analysis of survival from time of T cell transfer in mice bearing KB1P tumors (E) or MMTV-PyMT tumors (F) transplanted with $CD4^+$ T cells pre-treated *in vitro* with a vehicle control or with docetaxel. For E and F, p = values were determined using a log rank Mantel-Cox test in GraphPad Prism. See also Figure S5, Tables S1, and S2.

(Figures 3J and 3K). Additionally, we separated the CM into EV-enriched and EV-depleted fractions using a second method that involves serial ultracentrifugation steps, as previously described.[37] In this context, we again observed an induction of apoptosis in KB1P and MMTV-PyMT organoids treated with the EV-enriched fraction isolated from docetaxel-treated T cells compared to control T cells, while treatment with the EV-depleted fraction did not (Figure S5J). Lastly, we isolated the EV-enriched fraction from 118 × 10^9 docetaxel-treated human Jurkat T cells, and also confirmed the dose-dependent killing capacity of the EV-enriched fraction in human MDA-MB-231 tumor cells (Figure S5K). Interestingly, the amount of EVs required to induce similar levels of apoptosis appeared to be higher in the 2D MDA-MB-231 cell line compared to the mouse 3D tumor organoids (Figure S5K versus Figures 3H and 3I). Indeed, only the highest EV dose triggered a large induction of cell apoptosis (>25%) in the 2D cell line (Figure S5K) that is comparable to the 3D organoids setting (Figures 3H and 3I).

Tumor cells that gain the ability to grow as 2D cell lines have a decreased sensitivity to EV cytotoxicity

As outlined above, the ability of docetaxel-treated T cells to induce apoptosis seems more moderate in 2D cell lines than in 3D organoids. To experimentally validate this, we generated

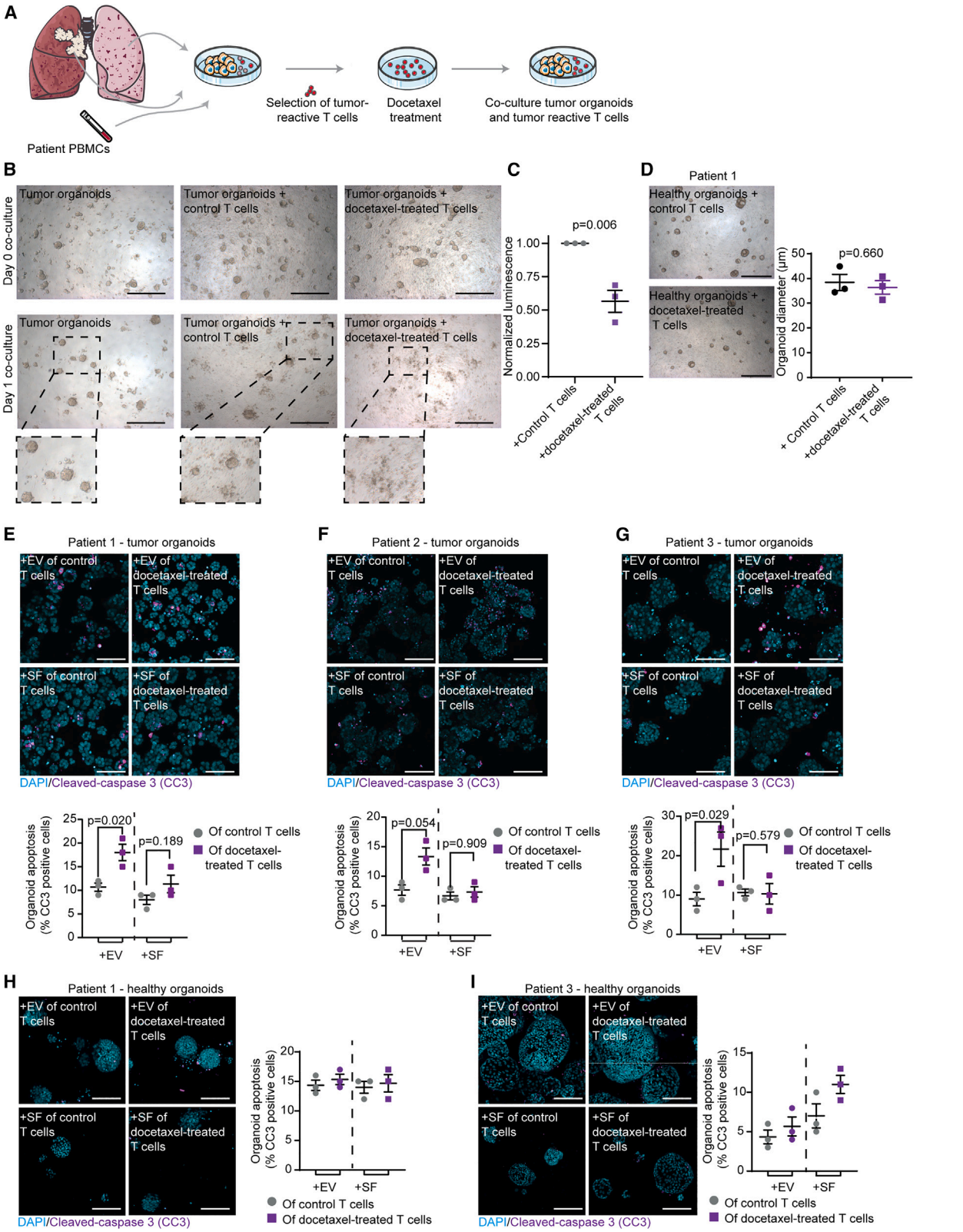

(legend on next page)

2D cell lines from the KB1P and MMTV-PyMT organoids. We noticed that during the generation of the 2D cell lines, dissociation of cells from the organoids and the BME, followed by culturing in 2D culture dishes, led to a large level of cell death, a process often referred to as anoikis.[38] Over time, a population of cells survived, which could be passaged as a 2D cell line, both for the KB1P and MMTV-PyMT models. Interestingly, we observed that compared to the corresponding 3D organoids, cell death occurring due to both low attachment plate/anoikis conditions (Figures 4A and 4B) and exposure to the EVs from docetaxel-treated T cells was reduced in those 2D cell lines (Figures 4C and 4D). To test whether the culture conditions caused the different sensitivity to anoikis and to EVs, we re-transferred the 2D cell lines into 3D BME to grow 3D organoid-like structures (from hereon named 2D-to-3D structures, Figures 4A and 4B). Strikingly, we observed that both the ability to survive in low attachment/anoikis conditions and the reduced response to EVs that we observed in the 2D cell lines were maintained in the 2D-to-3D structures (Figure 4), suggesting that these properties are stable regardless of the culture conditions. Collectively, tumor cells that gain the ability to grow as 2D cell lines become stably less sensitive to anoikis and to the cytotoxic properties of EVs released by docetaxel-treated T cells.

T cells pre-treated with docetaxel display therapeutic benefits *in vivo*

Over the years, several therapies based on T cells, including TILs or CAR T cells have been developed for clinical use for cancer. However, these therapies are based on TCR-mediated cytotoxicity, while we here show that docetaxel induces a non-canonical and TCR independent T cell cytotoxicity. We therefore next tested the ability of docetaxel to affect T cell-killing capacity in the context of tumor-specific T cells. For this purpose, we used again the OT I/OVA system, in which the TCRs of T cells are designed to recognized the OVA epitope[30,31] expressed here by the MMTV-PyMT OVA$^+$ organoids. As expected for TCR-mediated cytotoxicity, control OT I T cells induced apoptosis in MMTV-PyMT OVA$^+$ organoids (Figure 5A). Importantly, we observed that this cytotoxicity was further enhanced when OT I T cells were pre-treated with docetaxel (Figure 5A), demonstrating that docetaxel treatment has the potential to enhance T cell killing capacity also in tumor-specific T cells.

Next, we questioned whether adoptive transfer of docetaxel-treated T cells may have a therapeutic benefit. To test this, we isolated splenic T cells from healthy, non-tumor-bearing mice and pre-treated them with docetaxel for 72h as before. Subsequently, we intravenously injected a single dose of T cells into mice bearing KB1P or MMTV-PyMT tumors (Figure 5B). Strikingly, in mice that received docetaxel-treated T cells, we observed significantly slower tumor growth compared to mice that were injected with control T cells (Figures 5C and 5D). This demonstrated that T cells pre-treated with docetaxel *ex vivo* had the capacity to kill tumor cells growing *in vivo* and to halt tumor growth (Figures 5C and 5D). Moreover, monitoring tumor response showed that the anti-tumor capacity of T cells pre-treated with docetaxel appeared to be maintained for over ten days *in vivo*. Importantly, in both tumor models, a single transplantation of docetaxel-treated T cells resulted in a significant increase in mouse survival compared to the survival of mice that received control T cells (Figures 5E and 5F). We did not detect significant changes in the recruitment or activation of monocytes, tumor-associated macrophages (TAMs), dendritic cells, and neutrophils at 24h or 72h after transfer of docetaxel-treated T cells compared to control T cells (Figures S6A and S6B). This suggests that the strong therapeutic effect observed *in vivo* upon transfer of docetaxel-treated T cells may not be mediated by changes in intratumoral myeloid cells.

Collectively, pre-treating T cells *ex vivo* with docetaxel may be used to control tumor growth *in vivo* without the need to systemically administer docetaxel.

Docetaxel can further increase T cell cytotoxicity in material derived from patients with cancer

Lastly, we tested the ability of docetaxel to induce T cell-mediated killing in patient-derived tumor-reactive T cells. We previously generated a platform to obtain tumor-reactive patient-derived T cells and to study their interactions with matched patient-derived tumor organoids and healthy organoids.[39,40] We employed previously validated matched tumor-reactive T cells, autologous tumor organoids and autologous healthy lung organoids isolated from a patient with stage 2 (pT2bN1 with one lymph node metastasis) non-small cell lung cancer (NSCLC) to test whether docetaxel treatment of T cells could further increase their anti-tumor potential.[40] Tumor-reactive T cells were induced by culturing peripheral

Figure 6. Docetaxel increases T cell cytotoxicity via EV release in material derived from patients with cancer

(A) Schematic representation of establishment of patient-derived tumor organoids and tumor-reactive T cells.

(B) Representative images of co-cultures of human lung cancer organoids with matched tumor-reactive T cells pre-treated with a vehicle control or with docetaxel, at day 0 and day 1 of co-culture. Scale bar = 200 μm.

(C) Quantification of luciferase reporter activity in human lung tumor organoids after co-culture with tumor-reactive T cells pre-treated with a vehicle control or with docetaxel. n = 3 biological replicates with three technical repeats *per* replicate. Data are presented as mean ± SEM, p values were determined using unpaired, nonparametric t-test with a Mann-Whitney U correction in GraphPad Prism.

(D) Representative images and quantification of organoid diameter in co-cultures of human lung healthy organoids with matched tumor-reactive T cells pre-treated with a vehicle control or with docetaxel, at day 1 of co-culture. Scale bar = 200 μm. n = 3 biological replicates with three technical repeats *per* replicate. Data are presented as mean ± SEM, p-values were determined using unpaired, nonparametric t-test with a Mann-Whitney U correction in GraphPad Prism.

(E–G) Representative images and quantification of cleaved-caspase 3 (CC3) immunofluorescent staining in 3 patient-derived cancer organoids upon a 72h treatment with the extracellular vesicle (EV) and soluble fraction (SF) isolated from the conditioned media generated by tumor-reactive T cells treated with a vehicle control or docetaxel. n = 3 biological replicates, data are presented as mean ± SEM, p values were determined using unpaired, nonparametric t-test with a Mann-Whitney U correction in GraphPad Prism. Scale bar = 50 μm.

(H and I) Representative images and quantification of cleaved-caspase 3 (CC3) immunofluorescence staining in patient-derived lung healthy organoids (patient 1) and colon healthy organoids (patient 3) upon treatment with the EVs and the soluble fraction generated by tumor-reactive T cells treated with a vehicle control or with docetaxel. n = 3 biological repeats, scale bar = 50 μm, data are presented as mean ± SEM. p values were determined using unpaired, nonparametric t-test with a Mann-Whitney U correction in GraphPad Prism. See also Figure S6.

blood mononuclear cells (PBMCs) with autologous tumor organoids, as previously described[39,40] (Figure 6A). Subsequently, tumor-reactive T cells were pre-treated for 72h with 10 nmol/L of docetaxel, a dose that did not significantly alter T cell viability (Figures S6C and S6D). In addition, docetaxel did not increase the expression of CD137, CD107 or PD1 (Figures S6E–S6G). Moreover, we did not observe an increased secretion of IFNγ in docetaxel-treated T cells upon co-culture with tumor organoids (Figure S6H), confirming that docetaxel does not increase the ability of T cells to recognize tumor organoids and does not induce canonical T cell activation in this setting, in line with our findings in mouse T cells. Subsequently, we co-cultured tumor-reactive T cells with matched autologous cancer organoids and healthy organoids. Assessment of organoid viability following co-culture demonstrated that pre-treating T cells with docetaxel indeed increased their anti-tumor capacity against tumor organoids but not against healthy organoids (Figures 6B–6D).

Next, we asked whether patient-derived tumor-reactive T cells also release EVs with killing capacity upon treatment with docetaxel. We treated tumor-reactive T cells isolated from two patients with NSCLC (patient 1 and patient 2 with stage 4 disease) with control or docetaxel and we isolated the EV fraction and SF from the T cell CM. Subsequently, we exposed autologous tumor and healthy organoids to those fractions. Moreover, we treated tumor and healthy organoids isolated from a patient with stage 2 pT2N0 colorectal cancer (patient 3, for which we could not expand enough tumor-reactive T cells) with the EV fraction and SF of the tumor-reactive T cells of patient 2. In line with our observations in mouse T cells, we found in all three patient-derived material that EVs generated by tumor-reactive T cells treated with docetaxel triggered apoptosis in tumor organoids, while the SF did not (Figures 6E–6G). Moreover, apoptosis was not increased in healthy organoids upon treatment with the EV fraction or the SF (Figures 6H and 6I). Collectively, we find that docetaxel increases tumor-specific T cell killing in material from patients with cancer by inducing a release of cytotoxic EVs.

DISCUSSION

For decades, patients with cancer have been treated with taxanes; however, their efficacy remains sub-optimal in part due to the administration of low doses of taxanes to manage toxicity. The mode of action of taxanes *in vivo* has been contentious, and this has hindered the design of optimal treatment regimens. Although taxanes induce tumor cell death through mitotic perturbations *in vitro*,[21,22] they appear to exert their anti-tumor effects in *in vivo* cancer models and in patients with cancer through additional means.[4–7] For instance, taxanes have previously been suggested to alter the immunogenic properties of cancer cells[41,42] and to modulate macrophage cytotoxicity in rodents.[43,44] In this manuscript, we report an additional mode of action of taxanes *in vivo*, whereby docetaxel can trigger T cells to directly kill cancer cells by releasing EVs with cytotoxic properties. Interestingly, we find that cancer cells which are selected to grow as 2D cell lines become less sensitive to the cytotoxicity of these EVs. Strikingly, these cells also become less sensitive to induction of cell death in a low-atttachment/anoikis assay. This points to a potential link between sensitivity to anoikis and sensitivity to EV cytotoxicity, which warrants the future study of the induction of anoikis as one of the potential mechanisms of killing of cancer cells by taxane-treated T cells.

Most T cell therapies, including TILs or CAR T cells, are based on TCR-mediated T cell cytotoxicity. Indeed, T cell-mediated killing of target cells is classically thought to be supported by engagement of the TCR upon specific recognition of an antigen. However, other antigen-independent modes of killing by T cells have been described. For example, previous studies have reported that T cells can release cytokines at the cell periphery in addition to secretion at the immunological synapse, upon stimulation of IL-2R or IL-15R.[45,46] Moreover, a handful of studies have shown that T cells can release vesicles with cytotoxic properties.[47–49] Here, we demonstrate that treatment with taxanes can trigger T cells to release cytotoxic EVs and thereby induces T cell-mediated killing, independently of the TCR. Additionally, our data illustrate that the EVs released upon taxane treatment can further enhance T cell killing in the context of TCR-mediated cytotoxicity, both in mouse and patients with cancer. The release of EVs may be mediated by the microtubule-stabilization activity of docetaxel. Microtubules support the trafficking and release of cytokines and vesicles.[50] Indeed, upon stimulation of the TCR, T cells translocate their microtubule organizing center to the contact site, in order to polarize cytokine secretion and release of cytotoxic vesicles.[50–53] Future studies should address whether by stabilizing microtubules, docetaxel can bypass TCR activation to allow direct, untargeted release of cytotoxic EVs in the surrounding environment of T cells.

There are some limitations of the study. Firstly, our study reveals that EVs released by docetaxel-treated T cells trigger apoptosis in tumor cells, however we did not uncover the mechanism driving this process. Indeed, characterization of the content at the protein and RNA levels of EVs released by mouse naive T cells did not provide clear evidence of a particular mechanism of killing. Future work using either more sensitive screening techniques or other experimental T cell systems is required to understand the biological events leading to tumor cell death upon exposure to the EVs. Secondly, the correlation between response to EVs and sensitivity to anoikis remains to be further explored to elucidate whether and how EVs induce anoikis in recipient cells. In line with this, prior to clinical translation of our findings, further work is needed to reveal why healthy cells do not respond to taxane-treated T cells.

Prior studies have shown that taxanes can induce the release of EVs in other cell types including cancer cells.[54] However, the vesicles released by cancer cells displayed pro-metastatic properties,[54] and may therefore have a detrimental effect on cancer progression. Therefore, the here proposed strategy to treat T cells *ex vivo* with taxanes and to transfer them *in vivo* has the potential advantage to circumvent release of pro-metastatic EVs by cancer cells. Another advantage of *ex vivo* treatment of T cells with taxanes is that T cells are exposed to optimal doses of taxanes for 72h. By constrast, pharmacokinetic measurements have shown that the concentration of taxanes decreases rapidly in a time span of hours upon systemic treatment. In agreement with this, we observed that exposing T cells *ex vivo* to stable doses of taxanes for a prolonged period (72h) translates into a large therapeutic benefit upon a single transfer of docetaxel-treated T cells *in vivo*. Considering the relevance of our finding in clinical samples from patients with cancer, our study

has the potential to lead to the development of new T cell-based therapies, where T cells are treated *ex vivo* with optimal, stable doses of taxanes for maximized induction of EV release. Such a strategy can readily be applied to existing T cell therapies in order to boost their anti-tumor efficacy, in the context of both TCR-independent and TCR-mediated anti-cancer immunotherapies.

STAR★METHODS

Detailed methods are provided in the online version of this paper and include the following:

- KEY RESOURCES TABLE
- RESOURCE AVAILABILITY
  - Lead contact
  - Materials availability
  - Data and code availability
- EXPERIMENTAL MODEL AND STUDY PARTICIPANT DETAILS
  - Mouse models
  - Cell lines
  - Organoids and T cells from patients with cancer
  - Human breast tumor and healthy organoids
- METHOD DETAILS
  - Organoid culture and treatment
  - Generation and culture of 2D cell lines from mouse tumor organoids
  - Generation and culture of normal mouse mammary epithelial cells (MECs)
  - *In vivo* transplantation of tumor organoids and monitoring of tumor growth
  - Drug treatment *in vivo*
  - Flow cytometry isolation of T cells
  - Mouse T cell:organoid co-culture experiments
  - Virus production and transduction of organoids to express OVA
  - Generation of the Hela ABCB1 cells
  - Jurkat:human organoids and cell co-culture experiments
  - MTT assessment of mouse splenic T cell, Jurkat T cell and Hela cell survival following chemotherapy treatment *in vitro*
  - MTT assessment of organoid and cell survival following co-culture with T cells
  - Immunofluorescence staining of organoids and microscopy
  - Assessment of mouse T cell canonical activation
  - Screening for cytokine content in T cell supernatant
  - Immunohistochemistry
  - Quantification of cells with a mitotic plate
  - Time-lapse microscopy of co-cultures
  - Mass-spectrometry of conditioned media and extracellular vesicles
  - LC-MS/MS
  - Data analysis
  - T cell immunofluorescence staining and analysis
  - Isolation of extracellular vesicles and soluble fraction by size exclusion chromatography and treatment of tumor organoids and cell lines *in vitro*
  - Isolation of extracellular vesicles by ultracentrifugation
  - Electron microscopy and NanoSight particle analysis
  - Anoikis assay
  - Transfer of T cells in mice bearing tumors and characterization of myeloid cells in KB1P tumors
  - Experiments using material derived from patients with cancer
  - Tumor recognition assay
  - Tumor and healthy organoids killing assay
- QUANTIFICATION AND STATISTICAL ANALYSIS

SUPPLEMENTAL INFORMATION

Supplemental information can be found online at https://doi.org/10.1016/j.ccell.2023.05.009.

ACKNOWLEDGMENTS

The authors thank all members of the van Rheenen laboratory as well as Nathan Moldovan for critical reading of the manuscript. The authors also thank Felipe Rojas Rodriguez, Elzo de Wit, Amber Wezenaar, Maj Buchholz, the Pathology Department, the Animal Research facility and the Flow Cytometry facility of the Netherlands Cancer Institute for technical support. This manuscript was edited at Life Science Editors.

Funding: This work was supported by the Netherlands Organization of Scientific Research NWO (Vici grant 09150182110004, CancerGenomics.nl, and the Josef Steiner Cancer Research Foundation (JvR). CV is funded by a fellowship from the Human Frontiers in Science Program. The funders had no role in the study design; in the collection, analysis, and interpretation of data; in the writing of the paper; or in the decision to submit the paper for publication.

AUTHOR CONTRIBUTIONS

Conceptualization: C.V., D.M.P, E.E.V., S.C.L., and J.vR.

Methodology: C.V., C.M.C., L.B., S.L., H.G.J.D., T.S., S.V., S.R.B., R.M., L.Az, Validation: C.V., C.M.C., L.B., J.O.L., J.R.TvW., X.M., Formal analysis: C.V., C.M.C, X.M., J.O.L., J.R.T.vW., X.M., S.L., S.V., M.M., L.Az., R.M., Investigation: C.V., C.M.C., J.O.L., J.R.T.vW., X.M., S.L., S.V., E.T., H.G.J.D.

Resources: A.C.R., J.F.D., A.L.Z., D.M.P., E.E.V., S.L., M.I., A.A., L.Ak.

Writing –Original draft: C.V., E.P. and J.vR.

Writing – Review and editing: all authors.

Visualization: C.V., C.M.C., L.B., J.vR., Supervision: C.V., D.M.P., E.E.V., J.vR.

Project administration: C.V. and J.vR.

Funding acquisition: C.V. and J.vR.

DECLARATION OF INTERESTS

J.F.D. is named as inventor on a patent related to organoid technology. C.V., J.vR. and S.C.L. are named as inventors on a patent related to taxane treatment of T cells. The authors have no other competing interests to declare.

Received: April 11, 2022
Revised: February 28, 2023
Accepted: May 11, 2023
Published: June 12, 2023

REFERENCES

1. Jordan, M.A., and Wilson, L. (2004). Microtubules as a target for anticancer drugs. Nat. Rev. Cancer *4*, 253–265.
2. Early Breast Cancer Trialists' Collaborative Group EBCTCG (2019). Increasing the dose intensity of chemotherapy by more frequent administration or sequential scheduling: a patient-level meta-analysis of 37 298 women with early breast cancer in 26 randomised trials. Lancet *393*, 1440–1452.

3. Yvon, A.M., Wadsworth, P., and Jordan, M.A. (1999). Taxol suppresses dynamics of individual microtubules in living human tumor cells. Mol. Biol. Cell *10*, 947–959.

4. Milas, L., Hunter, N.R., Kurdoglu, B., Mason, K.A., Meyn, R.E., Stephens, L.C., and Peters, L.J. (1995). Kinetics of mitotic arrest and apoptosis in murine mammary and ovarian tumors treated with taxol. Cancer Chemother. Pharmacol. *35*, 297–303.

5. Janssen, A., Beerling, E., Medema, R., and van Rheenen, J. (2013). Intravital FRET imaging of tumor cell viability and mitosis during chemotherapy. PLoS One *8*, e64029.

6. Symmans, W.F., Volm, M.D., Shapiro, R.L., Perkins, A.B., Kim, A.Y., Demaria, S., Yee, H.T., McMullen, H., Oratz, R., Klein, P., et al. (2000). Paclitaxel-induced apoptosis and mitotic arrest assessed by serial fine-needle aspiration: implications for early prediction of breast cancer response to neoadjuvant treatment. Clin. Cancer Res. *6*, 4610–4617.

7. Milross, C.G., Mason, K.A., Hunter, N.R., Chung, W.K., Peters, L.J., and Milas, L. (1996). Relationship of mitotic arrest and apoptosis to antitumor effect of paclitaxel. J. Natl. Cancer Inst. *88*, 1308–1314.

8. Orth, J.D., Kohler, R.H., Foijer, F., Sorger, P.K., Weissleder, R., and Mitchison, T.J. (2011). Analysis of mitosis and antimitotic drug responses in tumors by in vivo microscopy and single-cell pharmacodynamics. Cancer Res. *71*, 4608–4616.

9. Maia, A.R.R., Linder, S., Song, J.Y., Vaarting, C., Boon, U., Pritchard, C.E.J., Velds, A., Huijbers, I.J., van Tellingen, O., Jonkers, J., and Medema, R.H. (2018). Mps1 inhibitors synergise with low doses of taxanes in promoting tumour cell death by enhancement of errors in cell division. Br. J. Cancer *118*, 1586–1595.

10. Zingoni, A., Fionda, C., Borrelli, C., Cippitelli, M., Santoni, A., and Soriani, A. (2017). Natural killer cell response to chemotherapy-stressed cancer cells: role in tumor Immunosurveillance. Front. Immunol. *8*, 1194.

11. Wargo, J.A., Reuben, A., Cooper, Z.A., Oh, K.S., and Sullivan, R.J. (2015). Immune effects of chemotherapy, radiation, and targeted therapy and opportunities for combination with immunotherapy. Semin. Oncol. *42*, 601–616.

12. Demaria, O., Cornen, S., Daëron, M., Morel, Y., Medzhitov, R., and Vivier, E. (2019). Harnessing innate immunity in cancer therapy. Nature *574*, 45–56.

13. Kersten, K., Salvagno, C., and de Visser, K.E. (2015). Exploiting the immunomodulatory properties of chemotherapeutic drugs to improve the success of cancer immunotherapy. Front. Immunol. *6*, 516.

14. Chen, G., and Emens, L.A. (2013). Chemoimmunotherapy: reengineering tumor immunity. Cancer Immunol. Immunother. *62*, 203–216.

15. Zitvogel, L., Apetoh, L., Ghiringhelli, F., and Kroemer, G. (2008). Immunological aspects of cancer chemotherapy. Nat. Rev. Immunol. *8*, 59–73.

16. Hodge, J.W., Garnett, C.T., Farsaci, B., Palena, C., Tsang, K.Y., Ferrone, S., and Gameiro, S.R. (2013). Chemotherapy-induced immunogenic modulation of tumor cells enhances killing by cytotoxic T lymphocytes and is distinct from immunogenic cell death. Int. J. Cancer *133*, 624–636.

17. Galluzzi, L., Buqué, A., Kepp, O., Zitvogel, L., and Kroemer, G. (2017). Immunogenic cell death in cancer and infectious disease. Nat. Rev. Immunol. *17*, 97–111.

18. Zhong, H., Han, B., Tourkova, I.L., Lokshin, A., Rosenbloom, A., Shurin, M.R., and Shurin, G.V. (2007). Low-dose paclitaxel prior to intratumoral dendritic cell vaccine modulates intratumoral cytokine network and lung cancer growth. Clin. Cancer Res. *13*, 5455–5462.

19. Kester, L., Seinstra, D., van Rossum, A., Vennin, C., Hoogstraat, M., van der Velden, D., Opdam, M., van Werkhoven, E., Hahn, K., Nederlof, I., et al. (2022). Differential survival and therapy benefit of breast cancer patients are characterized by distinct epithelial and immune cell microenvironments. Clin. Cancer Res. *28*, 960–971, in press.

20. Schmid, P., Adams, S., Rugo, H.S., Schneeweiss, A., Barrios, C.H., Iwata, H., Diéras, V., Hegg, R., Im, S.A., Shaw Wright, G., et al. (2018). Atezolizumab and nab-paclitaxel in advanced triple-negative breast cancer. N. Engl. J. Med. *379*, 2108–2121.

21. Nogales, E., Wolf, S.G., Khan, I.A., Ludueña, R.F., and Downing, K.H. (1995). Structure of tubulin at 6.5 A and location of the taxol-binding site. Nature *375*, 424–427.

22. Schiff, P.B., Fant, J., and Horwitz, S.B. (1979). Promotion of microtubule assembly in vitro by taxol. Nature *277*, 665–667.

23. Duarte, A.A., Gogola, E., Sachs, N., Barazas, M., Annunziato, S., R de Ruiter, J., Velds, A., Blatter, S., Houthuijzen, J.M., van de Ven, M., et al. (2018). BRCA-deficient mouse mammary tumor organoids to study cancer-drug resistance. Nat. Methods *15*, 134–140. https://doi.org/10.1038/nmeth.4535.

24. Lin, E.Y., Jones, J.G., Li, P., Zhu, L., Whitney, K.D., Muller, W.J., and Pollard, J.W. (2003). Progression to malignancy in the polyoma middle T oncoprotein mouse bresat cancer model provides a reliable model for human diseases. Am. J. Pathol. *163*, 2113–2126.

25. Ritsma, L., Vrisekoop, N., and van Rheenen, J. (2013). *In vivo* imaging and histochemistry are combined in the cryosection labelling and intravital microscopy technique. Nat. Commun. *4*, 2366.

26. Ciampricotti, M., Hau, C.S., Doornebal, C.W., Jonkers, J., and de Visser, K.E. (2012). Chemotherapy response of spontaneous mammary tumors is independent of the adaptive immune system. Nat. Med. *18*, 344–346. author reply 346.

27. Dou, J., Zhang, H., Liu, X., Zhang, M., and Zhai, G. (2014). In vitro and in vivo assessment of docetaxel formulation developed for esophageal stents. Collods Surf B Biointerfaces.

28. Davis, M.M., and Bjorkman, P.J. (1988). T-cell antigen receptor genes and T-cell recognition. Nature *334*, 395–402.

29. Burchat, A.F., Calderwood, D.J., Hirst, G.C., Holman, N.J., Johnston, D.N., Munschauer, R., Rafferty, P., and Tometzki, G.B. (2000). Pyrrolo [2,3-d]pyrimidines containing an extended 5-substituent as potent and selective inhibitors of lck II. Bioorg. Med. Chem. Lett. *10*, 2171–2174.

30. Hogquist, K.A., Jameson, S.C., Heath, W.R., Howard, J.L., Bevan, M.J., and Carbone, F.R. (1994). T cell receptor antagonist peptides induce positive selection. Cell *76*, 17–27.

31. Clarke, S.R., Barnden, M., Kurts, C., Carbone, F.R., Miller, J.F., and Heath, W.R. (2000). Characterization of the ovalbumin-specific TCR transgenic line OT-I: MHC elements for positive and negative selection. Immunol. Cell Biol. *78*, 110–117.

32. Montano, M. (2014). Model systems. In In Translational Biology in Medicine.

33. Sachs, N., de Ligt, J., Kopper, O., Gogola, E., Bounova, G., Weeber, F., Balgobind, A.V., Wind, K., Gracanin, A., Begthel, H., et al. (2018). A living biobank of breast cancer organoids captures disease heterogeneity. Cell *172*, 373–386.e10.

34. Dekkers, J.F., van Vliet, E.J., Sachs, N., Rosenbluth, J.M., Kopper, O., Rebel, H.G., Wehrens, E.J., Piani, C., Visvader, J.E., Verissimo, C.S., et al. (2021). Long-term culture, genetic manipulation and xenotransplantation of human normal and breast cancer organoids. Nat. Protoc. *16*, 1936–1965.

35. Lagas, J.S., Vlaming, M.L., van Tellingen, O., Wagenaar, E., Jansen, R.S., Rosing, H., Beijnen, J.H., and Schinkel, A.H. (2006). Multidrug resistance protein 2 is an important determinant of paclitaxel pharmacokinetics. Clin. Cancer Res. *12*, 6125–6132.

36. Böing, A.N., van der Pol, E., Grootemaat, A.E., Coumans, F.A.W., Sturk, A., and Nieuwland, R. (2014). Single-step isolation of extracellular vesicles by size-exclusion chromatography. J. Extracell. Vesicles *3*, 23430.

37. Zomer, A., Maynard, C., Verweij, F.J., Kamermans, A., Schäfer, R., Beerling, E., Schiffelers, R.M., de Wit, E., Berenguer, J., Ellenbroek, S.I.J., et al. (2015). *In Vivo* imaging reveals extracellular vesicle-mediated phenocopying of metastatic behavior. Cell *161*, 1046–1057.

38. Gilmore, A.P. (2005). Cell Death Differ. *12*, 1473–1477.

39. Cattaneo, C.M., Dijkstra, K.K., Fanchi, L.F., Kelderman, S., Kaing, S., van Rooij, N., van den Brink, S., Schumacher, T.N., and Voest, E.E. (2020). Tumor organoid-T-cell coculture systems. Nat. Protoc. *15*, 15–39.

40. Dijkstra, K.K., Cattaneo, C.M., Weeber, F., Chalabi, M., van de Haar, J., Fanchi, L.F., Slagter, M., van der Velden, D.L., Kaing, S., Kelderman, S., et al. (2018). Generation of tumor-reactive T cells by Co-culture of peripheral blood lymphocytes and tumor organoids. Cell *174*, 1586–1598.e12.

41. Hu, Y., Manasrah, B.K., McGregor, S.M., Lera, R.F., Norman, R.X., Tucker, J.B., Scribano, C.M., Yan, R.E., Humayun, M., Wisinski, K.B., et al. (2021). Paclitaxel induces micronucleation and activates pro-inflammatory cGAS-STING signaling in triple-negative breast cancer. Mol. Cancer Ther. *20*, 2553–2567.

42. Volk-Draper, L., Hall, K., Griggs, C., Rajput, S., Kohio, P., DeNardo, D., and Ran, S. (2014). Paclitaxel therapy promotes breast cancer metastasis in a TLR4-dependent manner. Cancer Res. *74*, 5421–5434.

43. Manthey, C.L., Perera, P.Y., Salkowski, C.A., and Vogel, S.N. (1994). Taxol provides a second signal for murine macrophage tumoricidal activity. J. Immunol. *152*, 825–831.

44. Burkhart, C.A., Berman, J.W., Swindell, C.S., and Horwitz, S.B. (1994). Relationship between the structure of taxol and other taxanes on induction of tumor necrosis factor-alpha gene expression and cytotoxicity. Cancer Res. *54*, 5779–5782.

45. Huse, M., Lillemeier, B.F., Kuhns, M.S., Chen, D.S., and Davis, M.M. (2006). T cells use two directionally distinct pathways for cytokine secretion. Nat. Immunol. *7*, 247–255.

46. Stinchcombe, J.C., Bossi, G., Booth, S., and Griffiths, G.M. (2001). The immunological synapse of CTL contains a secretory domain and membrane bridges. Immunity *15*, 751–761.

47. Cai, Z., Yang, F., Yu, L., Yu, Z., Jiang, L., Wang, Q., Yang, Y., Wang, L., Cao, X., and Wang, J. (2012). Activated T cell exosomes promote tumor invasion via Fas signaling pathway. J. Immunol. *188*, 5954–5961.

48. Peters, P.J., Geuze, H.J., Van der Donk, H.A., Slot, J.W., Griffith, J.M., Stam, N.J., Clevers, H.C., and Borst, J. (1989). Molecules relevant for T cell-target cell interaction are present in cytolytic granules of human T lymphocytes. Eur. J. Immunol. *19*, 1469–1475.

49. Peters, P.J., Borst, J., Oorschot, V., Fukuda, M., Krähenbühl, O., Tschopp, J., Slot, J.W., and Geuze, H.J. (1991). Cytotoxic T lymphocyte granules are secretory lysosomes, containing both perforin and granzymes. J. Exp. Med. *173*, 1099–1109.

50. Goodson, H.V., and Jonasson, E.M. (2018). Microtubules and microtubule-associated proteins. Cold Spring Harb. Perspect. Biol. *10*, a022608.

51. Finetti, F., Patrussi, L., Masi, G., Onnis, A., Galgano, D., Lucherini, O.M., Pazour, G.J., and Baldari, C.T. (2014). Specific recycling receptors are targeted to the immune synapse by the intraflagellar transport system. J. Cell Sci. *127*, 1924–1937.

52. Martín-Cófreces, N.B., Baixauli, F., and Sánchez-Madrid, F. (2014). Immune synapse: conductor of orchestrated organelle movement. Trends Cell Biol. *24*, 61–72.

53. Guedes-Dias, P., Nirschl, J.J., Abreu, N., Tokito, M.K., Janke, C., Magiera, M.M., and Holzbaur, E.L.F. (2019). Kinesin-3 responds to local microtubule dynamics to target synaptic cargo delivery to the presynapse. Curr. Biol. *29*, 268–282.e8.

54. Keklikoglou, I., Cianciaruso, C., Güç, E., Squadrito, M.L., Spring, L.M., Tazzyman, S., Lambein, L., Poissonnier, A., Ferraro, G.B., Baer, C., et al. (2019). Chemotherapy elicits pro-metastatic extracellular vesicles in breast cancer models. Nat. Cell Biol. *21*, 190–202.

55. Schipper, K., Seinstra, D., Paulien Drenth, A., van der Burg, E., Ramovs, V., Sonnenberg, A., van Rheenen, J., Nethe, M., and Jonkers, J. (2019). Rebalancing of actomyosin contractility enables mammary tumor formation upon loss of E-cadherin. Nat. Commun. *10*, 3800.

56. Conway, J.R.W., Warren, S.C., Herrmann, D., Murphy, K.J., Cazet, A.S., Vennin, C., Shearer, R.F., Killen, M.J., Magenau, A., Mélénec, P., et al. (2018). Intravital imaging to monitor therapeutic response in moving hypoxic regions resistant to PI3K pathway targeting in pancreatic cancer. Cell Rep. *23*, 3312–3326.

57. Vennin, C., Chin, V.T., Warren, S.C., Lucas, M.C., Herrmann, D., Magenau, A., Melenec, P., Walters, S.N., Del Monte-Nieto, G., Conway, J.R.W., et al. (2017). Transient tissue priming via ROCK inhibition uncouples pancreatic cancer progression, sensitivity to chemotherapy, and metastasis. Sci. Transl. Med. *9*, eaai8504.

STAR★METHODS

KEY RESOURCES TABLE

REAGENT or RESOURCE	SOURCE	IDENTIFIER
Antibodies		
Anti-mouse Cleaved-Caspase 3 (Asp175)	Cell Signaling Technology	9661; RRID: AB_2341188
Chicken anti-Rabbit Alexa Fluor 647	Thermo Fisher Scientific	9661; RRID: AB_2341188
Anti-mouse CD4	eBiosciences	14_9766_80; RRID: AB_2573007
Anti-mouse CD8	eBiosciences	14-0808; RRID: AB_2572860
anti-mouse CD4-eFluor660	eBioscience	50-0041-82; RRID: AB_10609337
anti-mouse CD8-eFluor660	eBioscience	50-0081-82; RRID: AB_10596646
Anti-mouse CD3	BD Bioscience	56-0033-80; RRID: AB_837092
Anti-mouse CD11b BV650	Biolegend	101259; RRID: AB_2566568
Anti-mouse F4/80-PE-Cy7	Biolegend	123113; RRID: AB_893490
Anti-mouse tubulin	Abcam	ab52866; RRID: AB_869989
Anti-mouse CD4 PE	Biolegend	100407; RRID: AB_312692
Alexa Fluor-488-conjugated Phalloidin	Thermo Fisher Scientific	12379; RRID: AB_10981332
Anti-mouse TNFα BB700	BD Bioscience	566510; RRID: AB_2869775
Anti-mouse Ki67 BV786	BD Bioscience	558615; RRID: AB_647130
Anti-mouse PD-1 BV421	BD Bioscience	562584; RRID: AB_2737668
Anti-mouse CD69 PE-DAZZLE	Biolegend	104535; RRID: AB_2565582
Anti-mouse FoxP3 AF488	Biolegend	126405; RRID: AB_1089114
Anti-mouse Ly6G APC	Biolegend	127613; RRID: AB_1877163
Anti-mouse Ly6C BV605	Biolegend	128035; RRID: AB_2562352
Anti-mouse CD11c-PE-Cy5.5	eBiosciences	35-0114-82; RRID: AB_469709
Anti-mouse CD103-PE/Dazzle	Biolegend	121429; RRID: AB_2566492
Anti-mouse PD-L1-PE	Biolegend	124307; RRID: AB_2073557
Anti-human PD-1 blocking antibody	Merus, the Netherlands	
Anti-human CD137-APC	BD Pharmingen	550890; RRID: AB_398477
Anti-human CD107a	BD Pharmingen	555801; RRID: AB_396135
Anti-human PD1	BD Horizon	566846
Anti-mouse Granzyme B Pacific Blue	Biolegend	515407; RRID: AB_2562195
Anti-mouse Perforin PE	Biolegend	1454305
Zombie Infra-Red	Biolegend	423105
Chemicals, peptides, and recombinant proteins		
Advanced Dulbecco's Modified Eagle Medium (DMEM) F/12 Glutamax	Thermo Fisher Scientific	12634028
Roswell Park Memorial Institute (RPMI) 1640	Thermo Fisher Scientific	21875034
DMEM/F12	Gibco	10565018
Dulbecco's modified Eagle's medium (DMEM)	Thermo Fisher Scientific	10564011
B27	Thermo Fisher Scientific	17504001
N-acetylcysteine	Sigma-Aldrich	A9165
Fetal Bovine Serum (FBS)	Thermo Fisher Scientific	A4766801
Cholera Toxin	Gentaur	MBS600443
EGF	Thermo Fisher Scientific	53003018
Insulin	Sigma Aldrich	I0516

(*Continued on next page*)

Continued

REAGENT or RESOURCE	SOURCE	IDENTIFIER
Cultrex PathClear Reduced Growth Factor Basement Membrane Extract Type 2	R&D Systems	3533-005-02
TryplE	Thermo Fisher Scientific	12605–010
Thiazolyl Blue Tetrazolium Bromide	Sigma Aldrich	298-93-1
Collagenase A	Roche	10103586001
HEPES	Thermo Fisher Scientific	15630106
Streptomycin/penicillin	Thermo Fisher Scientific	15140122
DNAse I	Roche	10104159001
DAPI	Thermo Fisher Scientific	D1306
Opti-MEM	Thermo Fisher Scientific	31985070
Polybrene	Sigma Aldrich	TR-1003-G
LCKi	Merck Millipore	213743-31-8
FGF	Thermo Fisher Scientific	PHG0261
Uranylacetate	Polysciences Inc	21447–25
Y-27632	Bio Connect	S1049
Ploy-D-lysine	Thermo Fisher Scientific	A3890401
Lipofectamine 2000	Thermo Fisher Scientific	11668019
Rimadyl (carpofen)	Zoetis	N/A
Temgesic (buprenorphine)	Indivior Europe Limited	N/A
Duratears	Alcon	N/A
*InVivo*MAb rat IgG2b isotype control, clone LTF-2	BioXCell	BE0090
*InVivo*MAb anti-mouse CD4, clone GK1.5	BioXCell	BE003-1
*InVivo*MAb anti-mouse CD8, clone YTS 169.4	BioXCell	BP0117
Fc block CD16/CD32, clone 2.4G2	BD Biosciences	553141
Permeabilization kit	eBioscience	00-5523-00
Golgi Plug	BD Biosciences	555029
Ultraglutamine	Lonza	BE17-605E/U1
PMA	Abcam	Ab120297
Ionomycin	MedChem Express	HY-13434
DAPI-containing Vectashield mounting medium	Vectorlab	H-1200-10
Foxp3 fixation/permeabilization buffer	eBioscience	00-5523-00
Sepharose CL-2B	GE Healthcare	17-0140-01
Critical commercial assays		
MycoAlert PLUS Kit	Lonza	LT07-118
LegendPlex Multi-Analyte Flow Assay kit for mouse Th Cytokine panel VbP VO3	BioLegend	741044
D-Luciferin	Promega	E1605
Experimental models: Cell lines		
Cell lines MDA-MB-231, HEP1, A375, RKO, RPE, HEK293T, Jurkat T cells and A549	ATCC	N/A
EGI-1 cell line DSMZ	DSMZ	N/A
HuH7 cell line CLS.	CLS	N/A
HeLa cell line	Gift from the Medema laboratory at the Netherlands Cancer Institute	N/A
U251-MG	Gift from Elly Hol	N/A

(*Continued on next page*)

Continued

REAGENT or RESOURCE	SOURCE	IDENTIFIER
Experimental models: Organisms/strains		
Mus musculus FVB/NRj	Janvier Labs	N/A
Mus musculus C57BL/6-Tg(TcraTcrb) 1100Mjb/J	The Jackson laboratory	003831
Mus musculus NOD/SCID/IL2r$\gamma^{-/-}$	The Netherlands Cancer Institute	N/A
Mus musculus FVB/NRj ROSA26^{mTmG}	The Netherlands Cancer Institute	N/A
Mus musculus K14-Cre; Brca1$^{fl/fl}$; p53 $^{fl/fl}$ (KB1P)	Described by Duarte et al., 2018.[23] Obtained from the group of Jos Jonkers at the Netherlands Cancer Institute	N/A
Mus musculus MMTV-PyMT	Described by Lin et al., 2003,[24] obtained from The Jackson laboratory	022974
Biological samples		
K14-Cre; Brca1$^{fl/fl}$; p53 $^{fl/fl}$ (KB1P) organoids	Described by Duarte et al., 2018[23]	N/A
MMTV-PyMT organoids	Described by Lin et al., 2003[24]	N/A
Organoids isolated from patients with breast cancer 13T; 27T; 38T; 62T; 100T; 169M; 36T	Described by Sachs et al., 2018[33] and Dekkers et al., 2021[34]	N/A
Healthy human breast organoids m12	Described by Sachs et al., 2018[33] and Dekkers et al., 2021[34]	N/A
Organoids isolated from patients with NSCLC or CRC	Described by Dijkstra et al., 2018[40] and Cattaneo et al., 2020[39]	N/A
T cells isolated from patients with NSCLC or CRC	Described by Dijkstra et al., 2018[40] and Cattaneo et al., 2020[39]	N/A
Recombinant DNA		
ABCB1 ORF	The Netherlands Cancer Institute	See Annex 2 for map
plv-OVA-mPlum	Gift from the Peeper lab, the Netherlands Cancer Institute	N/A
pLenti CMV Puro LUC	Addgene	w168–1; Plasmid #17477
psPAX2	Addgene	12260
PMD2.G	Addgene	12259
Software and algorithms		
FlowJo software 10.6.1	BD Biosciences	https://www.flowjo.com/
Fiji/ImageJ	https://imagej.net	2.1.0/1.53h
MaxQuant software 1.6.17.0	https://www.maxquant.org/	N/A
MetaMorph 7.10 software	Molecular Devices	N/A
Prism	GraphPad	9.0.0 (86)
Other		
Oasis HLB plate	Waters	WA31764.66
Ultimate 3000	Thermo Fisher Scientific	N/A
70 μm cell strainer	Corning	352350
0.22 μm cell strainer	Merck Millipore	SLGS033SS
Amilcon Ultra-15 10k column	Merck Millipore	UFC905024
Amilcon Ultra 2mL 10k column	Merck Millipore	UFC201024
Glass-bottom 96-well plate	Greiner bio-one	655076
24-well ultra-low adherence cluster polystyrene culture dish	Corning	4527
μ-Precolumn, 300μm i.d. x 5mmC18 PepMap100, 5 μm, 100 Å	Thermo Fisher Scientific	160454
Zeiss Axioskop2 Plus microscope	Carl Zeiss Microscopy, Jena, Germany	N/A
inverted research microscope Nikon Eclipse Ti-E	Nikon	N/A

(*Continued on next page*)

Continued

REAGENT or RESOURCE	SOURCE	IDENTIFIER
4k x 2.6k pixel CCD side-mounted camera	Modera, EMsis GmbH	N/A
Spinning disk Yokogawa CSU-X1-A1 with 405-491-561-642 quad-band mirror	Yokogawa	N/A
Prime BSI sCMOS camera	Photometrics	N/A
Four-laser Fortessa flow cytometer	Becton Dickinson	N/A
Leica TCS SP5 confocal microscope	Mannheim, Germany	N/A
FACSAria Fusion	BD Biosciences	N/A

RESOURCE AVAILABILITY

Lead contact

Further information and requests for resources and reagents should be directed to and will be fulfilled by the lead contact, Jacco van Rheenen (j.v.rheenen@nki.nl)

Materials availability

All materials used in this study are available upon request to the lead contact.

Data and code availability

The raw mass-spectrometry data is available via Pride (https://www.ebi.ac.uk/pride/) with the dataset identifier PXD041924. All data generated in this study are available upon request to the lead contact. We did not generate new code.

EXPERIMENTAL MODEL AND STUDY PARTICIPANT DETAILS

Mouse models

Experiments described in this manuscript were approved by the Animal Welfare Committee of the Netherlands Cancer Institute and were performed in accordance with national guidelines. All mice were housed in individually ventilated cage (IVC) systems under specific-pathogen-free conditions and received chow and water *ad libitum*. FVB/NRj females (Janvier), C57BL/6-Tg(TcraTcrb)1100Mjb/J females (OT I mice, Jackson laboratory), IL2r$\gamma^{-/-}$ females (Netherlands Cancer Institute) and ROSA26^{mTmG} FVB/NRj females (Netherlands Cancer Institute) were used at 8–10 weeks of age at the time of fat pad injection of tumor organoids and 8–20 weeks at the time of spleen isolation. Breast cancer organoids were derived from K14-Cre; Brca1$^{fl/fl}$; p53$^{fl/fl}$ mouse mammary tumors (KB1P[23]) and from MMTV-PyMT[24] mouse mammary tumors when mice had reached humane endpoint. MECs were isolated from 12- to 15- week-old female FVB/NRj mice.

Cell lines

Tumor cell lines MDA-MB-231, HEP1, A375, RKO, RPE, HEK293T, Jurkat T cells and A549 were obtained and authenticated from ATCC; EGI-1 line was obtained and authenticated from DSMZ. HuH7 was obtained and authenticated from CLS. U251-MG was a kind gift from Elly Hol. HeLa cells were obtained from the Medema Lab at the Netherlands Cancer Institute.

MDA-MB-231, A549, A375, U251-MG, EGI-1, HuH7, HEK293T, Hela and RKO cells were grown in DMEM GlutaMAX (Gibco, Cat. No. 31966047) containing FBS (10%, Thermo Fisher Scientific, Cat. No. A4766801) and Penicillin/streptomycin (1%, Thermo Fisher Scientific, Cat. No. 15140-122). HEP1 cells were grown in Roswell Park Memorial Institute (RPMI) 1640 Medium (Thermo Fisher Scientific, Cat. No. 21875034) containing FBS (10%, Thermo Fisher Scientific, Cat. No. A4766801) and Penicillin/streptomycin (1%, Thermo Fisher Scientific, Cat. No. 15140-122). RPE cells were cultured in DMEM/F12 GlutaMAX (Gibco, Cat. No 10565018) containing FBS (10%, Thermo Fisher Scientific, Cat. No. A4766801), Penicillin/streptomycin (1%, Thermo Fisher Scientific, Cat. No. 15140-122), and Ultraglutamine (1%, Lonza, Cat. No. BE17-605E/U1). Cells were kept in 20% O_2, 5% CO_2 and at 37°C and passaged ~twice a week using TrypLE (Thermo Fisher Scientific, Cat. No. 12605-010). Cells were routinely negatively tested for mycoplasma using the MycoAlert PLUS kit (Lonza, Cat. No. LT07-118).

Organoids and T cells from patients with cancer

Tumor organoids and T cells derived from patients with NSCLC and CRC

Written consent from all patients was obtained under the study NL48824.031.14, approved by the Medical Ethical committee of the Netherlands Cancer Institute. Isolation of tumor and healthy organoids, as well as T cells derived from patients with a confirmed diagnosis of NSCLC or colorectal cancer was previously described.[39,40] In brief, tumor tissue was isolated using a 18G core needle biopsy or during surgical resection. Next, tumor tissue was mechanically dissociated and enzymatically digested using 1.5 mg/mL collagenase II (Sigma-Aldrich), 10 μg/mL hyaluronidase type IV (Sigma-Aldrich) and 10 μmol/L Y-27632 (Sigma-Aldrich) before embedding in Geltrex. Organoids were regularly tested for mycoplasma contamination using the MycoAlert Mycoplasma Detection Kit (Lonza).

Patients' peripheral blood mononuclear cells (PBMC) were isolated by Ficoll-Paque density gradient separation of peripheral blood and cryopreserved until later use. For material from patients with cancer used for co-culture experiment with tumor reactive T cells and for treatment with EVs released by those T cells, the details are as follows. For patient 1 with NSCLC, the stage of the disease was stage 2 (pT2bN1 with one lymph node metastasis). For patient 2 with NSCLC, the stage of the disease was stage 4. Patient 3 had a stage 2 (pT2N0) colorectal cancer.

Human breast tumor and healthy organoids

The study protocol 12–427/C and the biobanking protocol HUB-Cancer TcBio#12–093 were approved by the medical ethical committee UMC Utrecht. All patients signed informed consent forms approved by the responsible authority. Tumor organoids from patients with breast cancer and from healthy donor was previously described.[33,34] Briefly, tumor tissue was mechanically and enzymatically digested in Advanced DMEM/F12 containing 1x Glutamax, 10 mmol/L HEPES and 1–2 mg/mL collagenase (Sigma, Cat. No. C9407) before embedding in type 2 BME. Breast tumor organoids identified with the code 13T, 27T, 62T and 100T were isolated from patients with Grade 3 ductal carcinoma with invasive growth. Breast tumor organoid line 36T was isolated from a patient with Grade 2 ductal carcinoma with invasive growth. Breast tumor organoid line 38T was isolated from patient with Grade 1 adenocarcinoma and breast tumor organoid line 169M was isolated from a patient with metastatic disease. Organoids were regularly tested for mycoplasma contamination using the MycoAlert Mycoplasma Detection Kit (Lonza).

METHOD DETAILS

Organoid culture and treatment

Mouse breast cancer organoids were derived from K14-Cre; Brca1$^{fl/fl}$; p53$^{fl/fl}$ mouse mammary tumors (KB1P[23]) and from MMTV-PyMT[24] mouse mammary tumors. Both lines were cultured in 50 μl drops of Cultrex PathClear Reduced Growth Factor Basement Membrane Extract Type 2 (BME, Amsbio, Cat. No. 3533-005-02). KB1P organoids were cultured in Advanced Dulbecco's modified Eagle's medium (adDMEM/F12; Thermo Fisher Scientific. Cat. No. 12634-010) containing Hepes (10 mmol/L; Thermo Fisher Scientific, Cat. No. 15630-056), Penicillin/streptomycin (1%, Thermo Fisher Scientific, Cat. No. 15140-122), B27 (2% Thermo Fisher Scientific, Cat. No. 17504-044), N-acetylcysteine (1.25 mmol/L; Sigma-Aldrich, Cat. No. A9165) and fibroblast growth factor (FGF, 12 ng/ml; Invitrogen, Cat. No. PHG0261). MMTV-PyMT organoids were cultured in DMEM/F12 GlutaMAX (Gibco, Cat. No 10565018) supplemented with 10 mmol/L Hepes (Gibco, Cat. No 15630106), Penicillin/streptomycin (1%, Thermo Fisher Scientific, Cat. No. 15140-122), B27 (2% Thermo Fisher Scientific, Cat. No. 17504-044) and fibroblast growth factor (FGF, 12 ng/ml; Invitrogen, Cat. No. PHG0261). Organoids were kept in 20% O_2, 5% CO_2 and at 37°C. Organoid cultures were routinely negatively tested for mycoplasma using the MycoAlert PLUS kit (Lonza, Cat. No. LT07-118). For passaging, organoids were split using TrypLE Express (Gibco, Cat. No. 12605010) while shaking for 10–15 min at 900 rpm and 37°C. For *in vitro* treatment, organoids were treated with doxorubicin (5 nmol/L) or its vehicle control PBS; docetaxel (5 nmol/L) or its vehicle control PBS and cyclophosphamide (5 μmol/L) or its vehicle control PBS.

Human CRC organoids were cultured in Advanced DMEM/F12 (Ad-DF+++; GIBCO) supplemented with 2 mmol/L Ultraglutamine I (Lonza), 10 mmol/L HEPES (GIBCO), 100/100 U/ml Pencillin/Streptomycin (GIBCO), 10% Noggin-conditioned medium, 20% R-spondin1-conditioned medium, 1x B27 supplement without vitamin A (GIBCO), 1.25 mmol/L N-Acetylcysteine (Sigma-Aldrich), 10 mmol/L nicotinamide (Sigma-Aldrich), 50 ng/mL human recombinant EGF (Peprotech), 500 nM A83-01 (Tocris), 3 μM SB202190 (Cayman Chemicals) and 10 nmol/L prostaglandin E2 (Cayman Chemicals). Human wild-type colon organoid medium is identical to CRC medium with the addition of 50% Wnt3a-conditioned medium. Human NSCLC and healthy organoid medium was composed of Ad-DF+++, 10% Noggin-conditioned medium, 10% R-spondin1-conditioned medium, 1x B27 supplement, 1.25 mmol/L N-Acetylcystein, 10 mmol/L nicotinamide, 25 ng/mL human recombinant FGF-7 (Peprotech), 100 ng/mL human recombinant FGF-10 (Peprotech), 500 nmol/L A83-01, 1 μmol/L SB202190, 5 μmol/L Y-27632.

Organoids derived from patients with breast cancer and from human milk were cultured in type 1 medium while milk-derived organoids were cultured in type 2 medium, which are described here.[34]

Generation and culture of 2D cell lines from mouse tumor organoids

KB1P and MMTV-PyMT 2D cell lines were generated by washing the BME out and dissociating tumor organoids in TrypLE Express (Thermo Fisher Scientific, Cat. No. 12605010) while shaking for 20 min at 37°C. Cells were next plated in 2D on plastic-bottom plates and were cultured in Dulbecco's modified Eagle's medium (DMEM, Thermo Fisher Scientific, Cat. No. 10564011) supplemented with FBS (10%, Thermo Fisher Scientific, Cat. No. A4766801), Penicillin/streptomycin (1%, Thermo Fisher Scientific, Cat. No. 15140-122), EGF (5 ng/ml, Thermo Fisher Scientific, Cat. No. 53003018) and Insulin (5 μg/ml, Sigma Aldrich, Cat. No. I0516) in 20% O_2, 5% CO_2 and at 37°C. Cells were kept in culture for a minimum of 10 days after being plated on plastic before functional assays, to remove cells that die during this process. 2D cells that were re-transferred into a 3D BME environment were kept in culture for the same duration before performing functional assays.

Generation and culture of normal mouse mammary epithelial cells (MECs)

MECs were isolated from 12- to 15- week-old female Friend Virus B mice, as previously described.[55] This matches the age of FVB mice from which tumors were isolated for preparing tumor organoids. MEC were cultured in BME and in DMEM/F12

(Gibco, Cat. No. 10565-018) containing fetal bovine serum (FBS, 10%, Thermo Fisher Scientific, Cat. No. A4766801), Penicillin/streptomycin (1%, Thermo Fisher Scientific, Cat. No. 15140-122), epidermal growth factor (EGF, 5 ng/ml; Peprotech, Cat. No. AF-100-15), insulin (5 ng/ml; Sigma, Cat. No. IO516-5ML) and cholera toxin (Gentaur, Cat. No. MBS600443). MECs were kept in 20% O_2, 5% CO_2 and at 37°C.

In vivo transplantation of tumor organoids and monitoring of tumor growth

For tumor generation, tumor organoids were transplanted into the 4th mammary fat pad of FVB female mice. Rimadyl (0.067 mg/ml, Zoetis) was administered to mice in the drinking water from 24h before surgery and for 48h after surgery. Mice were also treated with temgesic (0.1 mg/kg, Indivior Europe Limited), 1h before and 12h after surgery. Mice were anesthetized with isoflurane (2%, v/v) and their eyes were covered with duratears (Alcon). 100,000 single cells derived from KB1P organoids or 200,000 single cells derived from MMTV-PyMT organoids were injected in 30 μl of BME (Amsbio, Cat. No. 3533-005-02). Mice were weighed and monitored three times a week after transplantation of tumor organoids. Tumor volume was measured with calipers three times weekly. The researcher performing the measurement of tumor volume was blinded to the treatment group. For survival experiments, endpoint was reached when the tumor reached 1500 mm^3. Mice were sacrificed upon the humane endpoint. The schematic representations of treatment timelines are depicted in the figures of the manuscript.

Drug treatment *in vivo*

Once tumors were established and reached a size of ~7x7 mm, mice were randomized into treatment groups with the following drug dosages and timeline:

- AC + T treatment: every 14 days, cyclophosphamide (144 mg/kg, administered *via* intraperitoneal injection), doxorubicin (5 mg/kg, administered *via* intravenous injection) and docetaxel (25 mg/kg, resuspended in acetonitrile containing 0.1% acetic acid, administered *via* intravenous injection).
- AC treatment: every 14 days, cyclophosphamide (144 mg/kg, administered *via* intraperitoneal injection) and doxorubicin (5 mg/kg administered *via* intravenous injection).
- Docetaxel treatment: every 14 days, docetaxel (25 mg/kg, re-suspended in acetonitrile containing 0.1% acetic acid and administered *via* intravenous injections).
- Vehicle control for chemotherapy: every 14 days, the same volume of the vehicle as the corresponding chemotherapy was administered to mice. Vehicle for cyclophosphamide: saline; vehicle for doxorubicin: saline; vehicle for docetaxel: acetonitrile containing 0.1% acetic acid.
- IgG treatment: on day 1, day 3 and day 5 prior to treatment with vehicle control or with chemotherapy, treatment with 400 μg (day 1), or 200 μg (day 3 and day 5) *per* mouse with *InVivo*MAb rat IgG2b isotype control (BioXCell, clone LTF-2, Cat. No. BE0090).
- αCD4 treatment: on day 1, day 3 and day 5 prior to treatment with vehicle control or with chemotherapy, treatment with 400 μg (day 1), or 200 μg (day 3 and day 5) *per* mouse with *InVivo*MAb anti-mouse CD4 (BioXCell, clone GK1.5, Cat. No. BE003-1).
- αCD8 treatment: on day 1, day 3 and day 5 prior to treatment with vehicle control or with chemotherapy, treatment with 400 μg (day 1), or 200 μg (day 3 and day 5) *per* mouse with *InVivo*MAb anti-mouse CD8 (BioXCell, clone YTS 169.4, Cat. No. BP0117).

Flow cytometry isolation of T cells

Preparation of tissues

For isolation of T cells from mammary tumors, tumors were isolated, adjacent lymph nodes were removed and samples were mechanically dissociated using scalpel blades. Subsequently, enzymatic digestion of the tissue was performed in a mix containing collagenase A (3 mg/mL, Sigma Aldrich, Cat. No.10103578001) and DNAse (25 μg/ml, Sigma Aldrich, Cat. No. 10104159001), diluted in DMEM/F12 GlutaMAX (Gibco, Cat. No 10565018) containing FBS (10%), at 37°C for 1h in a rotating incubator. Samples were next filtered on a 70-μm cell strainer (Corning), washed in DMEM/F12 containing FBS (10%) and in FACS buffer (PBS, 5% FBS and 5 mmol/L EDTA). For isolation of T cells from the spleen of FVB female mice, the tissue was gently mechanically dissociated using a scalpel blade and glass slides.

Staining protocol

For both mammary tumors and spleen tissues, samples were next incubated in a red cell lysis buffer for 5 min at room temperature (NH4Cl 155 mmol/L, KHCO3 1 mmol/L, 0.1 mmol/L EDTA diluted in MilliQ water, pH=7.4). Subsequently, samples were blocked for 5 min at room temperature in a blocking buffer (FACS buffer containing 1:50 Fc block CD16/CD32 (BD Biosciences, Clone 2.4G2, Cat. No. 553141)). Next, samples were incubated with primary antibodies in the dark for 45 min at 4°C (anti-CD11b-BV650 (1:1200, BD Bioscience, clone M1/70, Cat. No. 563402); anti-CD4-PE (1:300, ThermoFisher, clone GK1.5, Cat. No. 12-0041-82) or anti-CD4-eFluor660 (1:300, BD Bioscience, clone GK1.5, Cat. No. 50-0041-82); and anti-CD8-eFluor660 (1:100, ThermoFisher, clone 53-6.7, Cat. No. 50-0081-82)). Samples were sorted on a Fusion Cell Sorter (Becton Dickinson). Gating strategies are depicted on Figures S1 and S2.

Mouse T cell:organoid co-culture experiments

Preparation of T cells

T cells isolated from mouse spleens or from mouse mammary tumors were cultured in Roswell Park Memorial Institute (RPMI) 1640 Medium (Thermo Fisher Scientific, Cat. No. 21875034) containing FBS (10%, Thermo Fisher Scientific, Cat. No. A4766801), Penicillin/streptomycin (1%, Thermo Fisher Scientific, Cat. No. 15140-122), IL-2 (150U/mL; Thermo Fisher Scientific, Cat. No. PMC0025), β-mercaptoethanol (50 μmol/L) and Ultraglutamine (2 mmol/L, Lonza, Cat. No. BE17-605E/U1). T cells were kept in 20% O_2, 5% CO_2 and at 37°C.

In order to assess the direct effects of docetaxel on T cell activation for T cells isolated from the spleen, T cells were cultured in the absence of CD3 and CD28 antibodies to avoid inducing classical T cell activation.

For T cells isolated from mouse mammary tumors, T cells were directly co-cultured with tumor organoids after FACS isolation. For T cells isolated from the spleen, T cells were treated for 72h with PBS or with docetaxel (10 nmol/L), in the presence or absence of an LCKi (10 μmol/L, Merck Millipore, Cat. No. 213743-31-8). To test the docetaxel-specificity of our observations, T cells were treated with paclitaxel 10 nmol/L or carboplatin 50 μmol/L for 72h. Subsequently, T cells were collected and washed 3 times in PBS to remove residual chemotherapy or LCKi.

Preparation of organoids

Tumor organoids or MECs grown in 3D BME were gently dissociated in TrypLE (Thermo Fisher Scientific, Cat. No. 12605-010) for 10 min at 37°C into small organoids (3–5 cells per organoids). Organoids and MECs were plated in 5 μl of BME in a 96-well plate.

T cells were added with a 1:3 ratio (T cell:tumor cell/MEC) in cell number. Cells were co-cultured in a 1:1 mix of T cell medium: organoid/MEC medium for 72h.

For treatment of organoids with conditioned medium generated by T cells, T cells were pre-treated with PBS or with docetaxel (10 nmol/L) for 72h. T cells were removed from the conditioned medium by centrifugation and the freshly isolated conditioned media were mixed with organoid medium (1:1 ratio) and added to the organoids for 72h.

Virus production and transduction of organoids to express OVA

For lentivirus production, 80% confluent human embryonic kidney (HEK) 293T cells were used in 10 cm dish (Greiner, Cat. No. 664160). Per dish, 7.5 μg of psPAX2, 2.5 μg PMD2.G and 10 μg of the plv-OVA-mPlum construct (gift from the Peeper lab at the Netherlands Cancer Institute) were mixed in 1 mL Opti-MEM (Thermo Fisher Scientific, Cat. No. 31985070). 40 μL lipofectamine 2000 (Thermo Fisher Scientific, Cat. No. 11668019) were added to the plasmid mix and incubated at room temperature for 15 min before being added to the HEK 293T cells. 18h later, the medium was refreshed with DMEM GlutaMAX (Thermo Fisher Scientific, Cat. No. 31966047) supplemented with streptomycin/penicillin (1%, Thermo Fisher Scientific, Cat. No. 15140122). After 48h, the medium was collected and filtered through a 0.22 μm filter (Millipore, Cat. No. SLGS033SS). Filtered medium was concentrated with an Amilcon Ultra-15 10k column (Millipore, Cat. No. UFC905024) for 1 h at 4,000 g. Breast cancer organoids isolated from a fully developed tumor in a MMTV-PyMT mouse with a C57BL/6NRj background were trypsinized into smaller clusters and incubated with 250 μL virus, 100 μg/mL polybrene (Sigma Aldrich, Cat. No. TR-1003-G) and 10 μmol/L Y-27632 (Bio Connect, Cat. No. S1049). Spin infection was done at 36°C, 600 g for 1 h and organoids were subsequently incubated at 37°C for 6 h. Next, organoids were washed twice with DMEM/F12 GlutaMAX medium (Thermo Fisher Scientific, Cat. No. 10565018) and plated in BME. Complete DMEM/F12 GlutaMAX medium (Thermo Fisher Scientific, Cat. No. 10565018), supplemented with 10 mmol/L Hepes (Thermo Fisher Scientific, Cat. No. 15630106), streptomycin/penicillin (1%, Thermo Fisher Scientific, Cat. No. 15140122), 10.08 ng/mL FGF (Thermo Fisher Scientific, Cat. No. PHG0261), B27 supplement (Thermo Fisher Scientific, Cat. No. 17504001) and 10 μmol/L Y-27632 (Bio Connect, Cat. No. S1049) was added to the organoids for 2 days. Organoids were selected with 0.5 μg/mL hygromycin (Thermo Fisher Scientific Cat. No. 10687-010).

Generation of the Hela ABCB1 cells

Hela cells (obtained from the Medema Lab at the Netherlands Cancer Institute) were transduced with a lentiviral overexpression construct of the ABCB1 ORF, with the sequence that can be found in Data S2 related to STAR Methods. The Hela ABCB1 cell line was derived by subsequent Taxol selection (100 nmol/L of Taxol).

Jurkat:human organoids and cell co-culture experiments

Preparation of Jurkat T cells

Jurkat T cells were cultured in Roswell Park Memorial Institute (RPMI) 1640 Medium (Thermo Fisher Scientific, Cat. No. 21875034) containing FBS (10%, Thermo Fisher Scientific, Cat. No. A4766801), Penicillin/streptomycin (1%, Thermo Fisher Scientific, Cat. No. 15140-122), and Ultraglutamine (2 mmol/L, Lonza, Cat. No. BE17-605E/U1). Jurkat T cells were kept in 20% O_2, 5% CO_2 and at 37°C.

Jurkat T cells were treated for 72h with PBS or with docetaxel (5 nmol/L) or with paclitaxel (5 nmol/L). Subsequently, Jurkat T cells were collected and washed 3 times in PBS to remove residual chemotherapy.

Jurkat T cells were added with a 2:1 ratio (T cell:tumor or healthy cell) in cell number. Organoids and cells were co-cultured with Jurkat T cells in a 1:1 mix of cancer/healthy organoids/cell medium:Jurkat cell medium for 72h.

MTT assessment of mouse splenic T cell, Jurkat T cell and Hela cell survival following chemotherapy treatment *in vitro*

100,000 T cells were seeded *per* well in a 96-well plate and treated with increasing doses of docetaxel, paclitaxel or carboplatin for 72h. Next, cells were incubated with Thiazolyl Blue Tetrazolium Bromide (0.5 mg/ml, Sigma Aldrich, Cat. No. 298-93-1) for 3 h in the dark at 37°C. Subsequently, cells were incubated for 16h in the dark in a lysis buffer (40% dimerhylformamide, 0.55 mol/L sodium dodecyl sulfate, 2% acetic acid, 8.4 mmol/L HCl in MilliQ water). Plates were read with a 565 nm wavelength.

MTT assessment of organoid and cell survival following co-culture with T cells

Following co-culture, medium was removed and cultures were washed in PBS to remove T cells. Organoids and cells were incubated with Thiazolyl Blue Tetrazolium Bromide (0.5 mg/ml, Sigma Aldrich, Cat. No. 298-93-1) for 3 h in the dark at 37°C. Subsequently, organoids and cells were incubated for 16h in the dark in a lysis buffer (40% dimerhylformamide, 0.55 mol/L sodium dodecyl sulfate, 2% acetic acid, 8.4 mmol/L HCl in MilliQ water). Plates were read with a 565 nm wavelength.

Immunofluorescence staining of organoids and microscopy

Organoids were fixed in 4% paraformaldehyde in PBS for 20 min at room temperature, followed by permeabilization in 0.2% TritonX-100 in PBS for 15 min at room temperature. A block was next performed in 5% Bovine Serum Albumin (BSA)/PBS for 2h at room temperature, followed by staining overnight at 4°C with anti-cleaved caspase 3 (1:200, Asp175, Cell Signalling, Cat. No. 9661). Appropriate Alexa Fluor labelled secondary antibody (Thermo Fisher Scientific) was combined with DAPI (1 μg/ml) and incubated for 2h in the dark at room temperature.

Images were acquired on an inverted Leica TCS SP5 confocal microscope (Mannheim, Germany), in 8 bit with a 20x dry immersion objective (HCX PL APO CS 20.0x0.70 DRY UV)). Fiji was used for quantification.

Assessment of mouse T cell canonical activation

Flow cytometry analysis

T cells isolated from the mouse spleen were treated with PBS or docetaxel (10 nmol/L) for 72h. For a positive control of canonical activation, some T cells were treated with 50 ng/ml PMA (Abcam, Cat. No. ab120297) and 1 μg/mL ionomycin (MedChem Express, Cat. No. HY-13434) for 3h at 37°C. T cells were then treated with a Golgi Plug (1:1000, BD Biosciences, Cat. No. 555029) at 37°C. Next, T cells were collected by centrifugation, washed in PBS 3 times and blocked for 5 min in FACS buffer containing 1:50 Fc block CD16/CD32 (BD Biosciences, Clone 2.4G2, Cat. No. 553141). T cells were then stained with cell surface markers (CD69-PE DAZZLE (Biolegend, Cat. No. 104536); Foxp3-AF488 (BD Bioscience, Cat. No. 567453); PD1-BV421 (BD Bioscience, Cat. No. 562584) at 4°C in the dark, washed with PBS and stained with a live/dead marker (Zombie InfraRed, 1:1000 in PBS) in the dark, at 4°C. Cells were washed in PBS, and permeabilized in a Foxp3 fixation/permeabilization buffer (eBioscience, Cat. No. 00-5523-00) for 30 min, in the dark and at 4°C. Next, cells were washed twice in permeabilization buffer (eBioscience, Cat. No. 00-5523-00), blocked for 5 min in FACS buffer containing 1:50 Fc block and stained with intracellular markers (Perforin-PE (BioLegend, Cat. No. 1454305), GranzymeB-Pacific Blue (GrzB, BioLegend, Cat. No. 515407), Ki67-BV786 (BD Bioscience, Cat. No. 563756), TNFα-BB700 (BD Bioscience, Cat. No. 566511)) for 30 min, in the dark at 4°C. Cells were washed in FACS buffer and analysed with a Becton Dickinson Fortessa. Acquired data were analyzed with FlowJo software.

Screening for cytokine content in T cell supernatant

T cells isolated from the spleen were treated with PBS or docetaxel (10 nmol/L) for 72h. For a positive control of canonical activation, some T cells were treated with 50 ng/ml PMA (Abcam, Cat. No. ab120297) and 1 μg/mL ionomycin (MedChem Express, Cat. No. HY-13434) for 3h at 37°C. Next, conditioned media were collected and T cells were removed by centrifugation. Cytokine content was assessed using the LegendPlex Multi-Analyte Flow Assay kit for mouse Th Cytokine panel VbP VO3 (BioLegend, Cat. No. 741044), as per the manufacturer's instruction. 650 μg of protein were resuspended in 25 μl for analysis. Each sample was measured in duplicate.

Immunohistochemistry

Tumors were collected and fixed in EAF (ethanol/acetic acid/formaldehyde/saline at 40:5:10:45 v/v) and embedded in paraffin. Next, 4 μm-thick sections were stained with CD4 (eBiosciences, Cat. No. 14_9766_80) or CD8 (eBiosciences, Cat. No. 14–0808). The stained sections were reviewed with a Zeiss Axioskop2 Plus microscope (Carl Zeiss microscopy, Jena, Germany).

Quantification of cells with a mitotic plate

Cells with a mitotic plate were identified on Hematoxylin and Eosin stained sections, based on nuclear condensation and cellular shape, as previously performed.[56,57] For each tumor, 10 fields of view (FOV) were analyzed and the number of cells with a mitotic plate *per* FOV was plotted.

Time-lapse microscopy of co-cultures

T cells and KB1P organoids were co-cultured as described above. Images were acquired on a Leica SP5 confocal microscope (Mannheim, Germany) in 12-bit with a 20x dry immersion objective (HCX PL APO CS 20.0x0.70 DRY UV). Time-lapse imaging was analyzed using Zeiss software and ImageJ software.

Mass-spectrometry of conditioned media and extracellular vesicles

T cells isolated from the mouse spleen were treated with PBS or docetaxel (10 nmol/L) for 72h, in the absence of FBS. For analysis of the conditioned media, conditioned media were collected and T cells were removed by centrifugation.To analyse the proteins contained in EVs, EVs were isolated using sepharose beads, as described in the relevant Method sub-section of this manuscript. For each repeat, we isolated the EVs released by 6x10^6 T cells treated with PBS or with docetaxel. Samples were processed for mass-spectrometry as follows. Proteins in the conditioned media were precipitated with subsequent addition of 4x (v/v) MeOH, 1x (v/v) CHCl3 and 3x (v/v) MQ. The protein pellet was resuspended in digestion buffer, containing 1% SDC, 100 mmol/L Tris pH 8.5, 5 mmol/L Tris(20carboxyethyl)phosphine (TCEP) and 30 mmol/L CAA. Trypsin (1:50) and LysC (1:100) were added and proteins were digested overnight at 37°C. Digestion was terminated and SDC was precipitated by addition of 10% FA to a final concentration of 0.5% FA (v/v). SDC was removed by centrifugation. Peptides were desalted using Oasis HLB plates (Waters).

LC-MS/MS

Microflow LC-MS/MS was performed using an Ultimate 3000 (Thermo Fisher Scientific, Bremen, Germany) coupled to an Orbitrap Exploris™ 480. Lyophilized phosphopeptides were resuspended in 1 % (v/v) formic acid and injected, trapped and washed on a trap-column (μ-Precolumn, 300μm i.d. x 5mmC18 PepMap100, 5 μm, 100 Å (Thermo Scientific, Cat. No. 160454)) for 5 min at a flow rate of 5 μL/minute with 92% buffer A (0.1 FA, in HPLC grade water). Peptides were subsequently transferred onto an analytical column (75μm x50 cm Poroshell 120 EC-C18, 2.7μm, Agilent Technology, packed in-house) and separated at 40°C at a flow rate of 0.3 μl/min using a 175 min (for conditioned media samples) or a 90 min (for EVs) linear gradient from 9% to 36% buffer B (0.1% FA, 80% ACN). Electrospray ionization was performed using 1.9kV spray voltage and a capillary temperature of 275°C. The mass spectrometer was operated in data-dependent acquisition mode: full scan MS spectra (m/z 375 – 1,600) were acquired in the Orbitrap at 60,000 resolution for a maximum injection time set to auto-mode with a standard AGC target. High resolution HCD MS2 spectra were generated using a normalized collision energy of 28%. MS2 scans were acquired in the Orbitrap mass analyzer at a resolution of 30,000 (isolation window of 1.4Th) with a standard AGC target and an automatic maximum injection time. Precursor ions with unassigned charge state as well as charge state of 1+ or superior/equal to 6+ were excluded from fragmentation.

Data analysis

Raw files were processed using MaxQuant software (version 1.6.17.0) and the Andromeda search engine was used to search against *Mus Musculus* database (Uniprot reviewed, 17090 entries) with the following parameters: trypsin digestion with a maximum of 2 missed cleavages, carbamidomethylation of cysteines (57.02 Da) as a fixed modification and methionine oxidation (15.99 Da) as variable modification. Mass tolerance was set to 4.5 ppm at the MS1 level and 20 ppm at the MS2 level. The False Discovery Rate (FDR) was set to 1% for peptide-spectrum matches (PSMs) and protein identification using a target-decoy approach, minimum peptide length was set to 7 residues. Relative label-free quantification was performed using the MaxLFQ algorithm with the minimum ratio count set to 2. LFQ intensities were log2 transformed and only proteins with at least two valid values in each conditions were considered. Relative label-free quantification was performed using iBAQ algorithm, intensities were log2 transformed and only proteins with at least two valid values were considered.

T cell immunofluorescence staining and analysis

Mouse T cells isolated from the spleen and treated with a vehicle control or with docetaxel (10 nmol/L for 72h) were seeded on glass coverslips pre-coated with poly-D-lysine (Thermo Fisher Cat. No. A3890401) and with αCD3 (eBioscience, Cat. No. 56-0033-80) for 15 min. Next, for immunofluorescence staining of tubulin, cells were extracted for 1 min with pre-warmed (37°C) extraction buffer composed of MRB80 (80 mmol/L K-PIPES pH 6.8, 4 mmol/L MgCl2, 1 mmol/L EGTA) supplemented with 0.35% Triton X-100 and 0.2% glutaraldehyde, followed by fixation using pre-warmed (37°C) 4% paraformaldehyde (PFA) in PBS for 10 min. Cells were washed with PBS and permeabilized with 0.2% Triton X-100 in PBS for 5 min. Epitope blocking and antibody labeling steps were performed in PBS with 3% BSA. After staining and washing with PBS, cells were air dried and mounted in DAPI-containing Vectashield mounting medium (Vector Laboratories, Cat. No. H-1200-10). The following primary antibody was used: rabbit anti-tubulin (clone EP1332Y, Abcam, Cat. No. ab52866). Secondary antibody was highly cross-adsorbed Alexa Fluor-594-conjugated goat anti-rabbit IgG (Thermo Fisher Scientific). For labeling of actin, Alexa Fluor-488-conjugated Phalloidin (Thermo Fisher Scientific, Cat. No. 12379) was included during secondary antibody incubation. STED imaging was performed using a Leica TCS SP8 STED 3X microscope equipped with a HC PL Apo 100x/1.40 Oil STED WHITE objective. A pulsed white laser (80 MHz) was used for excitation, and a 775 nm pulsed depletion laser was used. The internal Leica GaAsP HyD hybrid detectors were used with a time gate of $1 \leq tg \leq 6$ ns. The set-up was controlled using LAS X.

For fluorescence intensity quantifications, samples were imaged on a spinning disk confocal setup consisting of an inverted research microscope Nikon Eclipse Ti-E (Nikon) equipped with the perfect focus system (Nikon), Plan Apo VC 100x N.A. 1.40 oil objective (Nikon), spinning disk Yokogawa CSU-X1-A1 with 405-491-561-642 quad-band mirror (Yokogawa). The system was equipped with an ASI motorized stage with piezo plate MS-2000-XYZ (ASI), Prime BSI sCMOS camera (Photometrics) and controlled by the MetaMorph 7.10 software. For excitation, 405 nm 100 mW Stradus (Voltran), 491 nm 100 mW Calypso (Cobolt), and 561 nm 100 mW Jive (Cobolt) lasers were used in combination with ET-BFP2 (49021, Chroma), ET-GFP (49002, Chroma), and ET-mCherry (49008, Chroma) filter sets, respectively. Z-stacks of cells were acquired with a step size of 0.25 μm.

All images were processed using ImageJ. For quantification of fluorescence intensity, sum projections were made for each z stack using ImageJ. Next, the raw integrated density of a square box around individual cells of interest per image, as well as an empty region in the field of view, were calculated using ImageJ. Per image, the background intensity from the empty region was subtracted from the measured integrated density for each cell in the field of view to give the background corrected intensity per cell.

Isolation of extracellular vesicles and soluble fraction by size exclusion chromatography and treatment of tumor organoids and cell lines *in vitro*

T cells isolated from the mouse spleen or tumor-reactive T cells from patients with NSCLC[39,40] were treated with PBS or docetaxel (10 nmol/L) for 72h. Next, conditioned media were collected and T cells were removed by centrifugation. Conditioned media were spun twice at 500g for 10 min and twice at 2000g for 15 min at 4°C. For isolation of extracellular vesicles (EVs), Sepharose CL-2B (GE Healthcare, Cat. No. 17-0140-01) were first washed in PBS. Next, columns were prepared by adding a nylon panty hose into the outlet of a syringe. Sepharose was next stacked into the column and allowed to settle until 10 ml of stacked column was reached. Subsequently, 1.5 ml of conditioned medium were carefully added to the column and sample collection of fractions of 0.5 ml started immediately. When the conditioned medium had entered the Sepharose, a few drops of PBS were added progressively. Once the PBS had entered the Sepharose, more PBS was added until filling the column entirely. PBS was continuously added during the collection of all fractions. Fractions 9 and 10 contain the majority of EVs with a high purity, fractions 20 and 21 contain the majority of proteins and high-density lipoproteins. Next, collected fractions were loaded onto Amicon Ultra 2 ml columns with a 10 kDa cut off (Merck, Cat. No. UFC201024). Fractions were centrifugated at 3,000 g for at least 10 min and samples were recovered by placing the filter unit upside down and centrifugating at 1,000 g for 2 min. Following isolation, EV fractions and soluble fractions were kept in −80°C conditions until functional assays. Each sample was resuspended in a specific volume to normalize the EV fraction or soluble fraction concentration to the initial number of T cells from which they were derived. To test the killing ability of EVs, tumor organoids and 2D-to-3D structures were seeded in 5 μl of BME and 2D tumor cells were seeded on a glass-bottom 96-well plate (Greiner-BioOne, Cat. No. 655076). Except for the dose response in MDA-MB-231 (Figure S5K), organoids and cells were treated with the EV fraction or with the soluble fraction at a 1:10 dilution in organoid or cell media. Mouse cancer organoids (3D and 2D-to-3D) and cancer cells (2D) (KB1P and MMTV-PyMT) were treated with EVs released by 6-8x10^6 T cells; patient-derived tumor organoids were treated with EVs released by 7x10^6 patient-derived tumor reactive T cells. 72h after the initiation of treatment with EVs, cultures were washed and fixed for immunohistochemical assessment of cleaved-caspase 3.

Isolation of extracellular vesicles by ultracentrifugation

T cells isolated from the mouse spleen or Jurkat T cells were treated with PBS or with docetaxel (10 nmol/L and 5 nmol/L, respectively) for 72h. Subsequently, conditioned media were collected and T cells were removed by centrifugation at 1500g for 5 min. Next, conditioned media were spun twice at 500g for 10 min and twice at 2000g for 15 min, at 4°C. Subsequently, the EVs were isolated as previously described.[37] Supernatant was centrifuged twice at 16,500g for 20 min. The supernatant was next spun at 100,000g for 1h. Afterwards, the supernatant (containing soluble factors without the EVs) was removed and concentrated using Amicon Ultra columns with a 10 kDa cut off (Merck, Cat. No. UFC201024). These samples are the 'EV-depleted fraction'. The pellets obtained after the first centrifugation at 100,000g were pooled and centrifuged once more at 100,000g for 1h. The resulting pellets containing the EV-enriched fractions were resuspended in PBS and concentrated using Amicon Ultra 2 ml columns with a 10 kDa cut off (Merck, Cat. No. UFC201024). The EV-enriched and EV-depleted fractions were kept at −80°C until further use. Each sample was resuspended in a specific volume to normalize the sample concentration to the initial number of T cells from which they are derived.

Electron microscopy and NanoSight particle analysis

For electron microscopy measurements, EV fractions derived from mouse T cells and obtained using sepharose beads were spotted on carbon/formvar-coated mesh grids. After blotting off the excess liquid, the samples were contrasted by 2% uranylacetate (Polysciences Inc, Cat. No. 21447-25) in water for 1 minute, the excess stain was blotted off and grids was air dried. Vesicular structures were imaged in a 60 kV JEOL1010 (JEOL) TEM at 60,000x magnification using a 4k x 2.6k pixel CCD side-mounted camera (Modera, EMsis GmbH).

The distribution of EV diameter was analyzed using a NanoSight. The measurements report the tracking of Brownian motion of individual nanoparticles detected by scattered light, as a function of temperature and dispersing medium viscosity.

Anoikis assay

Response to anoikis was determined by seeding cells at a density of 30,000 cells per 500ul of culture medium in a 24-well ultra-low adherence cluster polystyrene culture dish (Corning, Cat. No. 4527). 48h later, cells were harvested and resuspended in 100 μl of PBS containing DAPI. Signals were acquired on a four-laser Fortessa flow cytometer (Becton Dickinson) and analyzed on FlowJo software.

Transfer of T cells in mice bearing tumors and characterization of myeloid cells in KB1P tumors

$CD4^+$ T cells were isolated from the spleen of non-tumor bearing, untreated FVB female mice, based on DAPI-/$CD11b^-$/$CD4^+$ expression. T cells were treated *in vitro* with PBS or docetaxel (10 nmol/L) for 72h. Subsequently, T cells were washed three times in PBS to

remove residual docetaxel and 2x10^6 T cells resuspended in 100 μl HBSS were transferred by intravenous injections into tumor-bearing mice. Importantly, tumors at the time of intravenous transfer of T cells had a size between 100 mm^3 and 250 mm^3. Transfer of docetaxel-treated T cells into mice bearing larger tumors (>300 mm^3) led to mouse death shortly after T cell transfer. Histopathological analysis did not reveal significant tissue damage in those mice, therefore the cause of death was not identified. Transfer of control T cells in mice bearing large tumors never led to mouse death.

For Figures S6A and S6B, 24h and 72h after transfer of T cells, mice were sacrificed and tumors were collected. The lymph nodes were removed and tumors were minced and digested for 45 min at 37°C in DMEM/F12 GlutaMAX containing 0.2% trypsin and 0.2% collagenase A (Sigma-Aldrich, Cat. No. 101035860001). Next, tumors were blocked in FACS buffer containing Fc block CD16/CD31 (1:50; BD Biosciences, Clone 2.4G2, Cat. No. 553141) for 20 min, at room temperature. Subsequently, samples were stained with extracellular antibodies for 30 min in the dark, at 4°C: (Ly6C-BV605 (1:600; BD Biosciences, Cat. No. 755205); CD11b-BV421 (1:1200, Biolegend, Cat. No. 566313); F4/80-PE-Cy7 (1:400, Biolegend, Cat. No. 123113); CD11c-PE-Cy5.5 (1:400, eBiosciences, Cat. No. 35-0114-82), CD103-PE/Dazzle (1:200, Biolegend, Cat. No. 121429); PDL1-PE (1:400, Biolegend, Cat. No. 124307); CD45-AF700 (1:200, Biolegend, Cat. No. 103127), Ly6G-APC (1:150, Biolegend, Cat. No. 127613). Next, samples were stained with Zombie NIR for 15 min in the dark at 4°C before being permeabilized and fixed using a permeabilization kit (Thermo Fisher Scientific, Cat. No. 00-5523-00) according to the manufacturer's guidelines. Samples were then stained with intracellular antibody (Ki67-BV786, 1:200, BD Bioscience, Cat. No. 563756). Signals were acquired on a four-laser Fortessa flow cytometer (Becton Dickinson) and analyzed on FlowJo software.

Experiments using material derived from patients with cancer

Generation of tumor organoids reactive PBMC

Tumor-reactive patient T cells were generated by co-culturing PBMCs and autologous tumor organoids as described previously.[39,40] In brief, following incubation with 200 ng/ml IFNγ for 24 h, patient tumor organoids were dissociated into single cell suspensions using TripLE Express. Tumor organoid cells were mixed with patient PBMCs (20:1 tumor cell/PBMC ratio) and 10^5 cells were seeded in each well of a U-bottom 96-well plate pre-coated with 5 μg/ml αCD28 antibody. Co-culture medium consisted of RPMI 1640 supplemented with 2 mmol/L Ultraglutamine I, 1% penicillin/streptomycin, 10% human AB serum, 150 U/ml rh-IL-2 and 20 μg/ml αPD-1 blocking antibody (kindly provided by Merus, The Netherlands). Medium, IL-2 and αPD-1 were refreshed every 2–3 days. PBMCs were harvested and re-stimulated every 7 days by re-plating with fresh tumor organoid cells. After two weeks of co-culture, PBMCs were harvested and used for downstream analysis or cryopreserved for later use.

Tumor recognition assay

Tumor-reactive PBMC were thawed in pre-warmed T cells medium and incubated for 15 min with 25 U/mL Benzonase. After washing, cells were re-suspended at 2–3×10^6 cells/ml in T cell medium and cultured overnight at 37°C. T cell medium consisted of RPMI 1640 supplemented with 2 mmol/L Ultraglutamine I, 1% penicillin/streptomycin, 10% human AB serum and 150 U/ml rh-IL-2. The day after, PBMC were incubated with (or without) 10 nmol/L docetaxel for 48 h.

For evaluation of tumor reactivity, 10^5 PBMCs were re-stimulated with autologous tumor organoids or autologous healthy organoids (isolated from Geltrex for 48h and stimulated with 200 ng/ml IFNγ for 24h, as described in[39,40]) at a 2:1 effector:target ratio and seeded in αCD28 coated plates in the presence of 20 μg/ml αPD-1 and co-cultured for 24 hours. At the end of the 24h, 50 μl of the assay supernatant were taken on the side and used for the quantification of the secreted IFNγ. To this purpose, the Human IFN-γ Flex Set (BD bioscience) was used in accordance with the manufacturer's instructions.

For the evaluation of CD137, CD107a and PD-1 expression, at the end of the 24h, cells were washed twice in FACS buffer and stained with the following antibodies: αCD3 PerCPCy5.5, αCD4 FITC, αCD8 BV421, αCD137 APC (BD Pharmingen, Cat. No. 550890), αCD107a (BD Pharmingen, Cat. No. 555801), αPD-1 (BD Horizon, Cat. No. 566846) and nearIR viability dye for 30 min at 4°C in the dark. PBMCs stimulated with 50 ng/ml PMA (Sigma Aldrich) and 1 μg/ml ionomycin (Sigma Aldrich) served as positive controls and PBMCs cultured without tumor stimulation as negative controls. Cells were then washed twice with FACS buffer and recorded with a Becton Dickinson Fortessa or LSRII flow cytometer.

Tumor and healthy organoids killing assay

To express luciferase in the tumor organoids, we used pLenti CMV Puro LUC (w168–1; Plasmid #17477; Addgene).

Tumor-reactive PBMC were thawed in pre-warmed T cell medium and incubated for 15 min with 25 U/ml Benzonase. After washing, cells were re-suspended at 2–3×10^6 cells/ml in T cell medium and cultured overnight at 37°C. The day after, PBMC were incubated with (or without) 10 nmol/L docetaxel for 48 h.

To determine the sensitivity of tumor and healthy organoids to T cell–mediated killing, flatbottom non-tissue culture treated plates were coated with 5 μg/ml αCD28 and kept at 4°C overnight prior to co-culture. Tumor organoids were previously transduced with luciferase reporter gene. Organoids were isolated from Geltrex 48 hours prior to co-culture and stimulated with 200 ng/ml IFNγ for 24 h prior to co-culture. The next day, part of the organoids were dissociated to single cells and counted using a hemocytometer. This was used to infer the number of tumor cells *per* tumor organoid to allow co-culture of organoids and T cells at a 5:1 effector:target ratio. Next, organoids and tumor reactive T cells were resuspended in the T cell medium. αCD28 coated plates were washed twice with PBS and 10^4 organoids were seeded for 72 h in triplicate without T cells or with 5x10^4 autologous tumor-reactive T cells (incubated or not with docetaxel). At the end of the 72 hours, tumor and healthy organoids viability in the different conditions was evaluated

by microscopy, taking bright-field pictures at 5 and 10X magnification. Tumor cell viability in the different conditions was also measured by luciferase reporter assay using 3 μg/mL luciferin. Luminescence was measured with a Tecan reader (1,000 ms exposure).

QUANTIFICATION AND STATISTICAL ANALYSIS

Unless stated otherwise in the figure legends, p-values were determined using unpaired, nonparametric t-test with a Mann-Whitney U correction in GraphPad Prism. Kaplan Meier survival curves were analyzed with a log-rank Mantel-Cox test in GraphPad Prism. Statistical analysis of tumor growth depicted in Figure 5D was performed in Prism GraphPad using a mixed-effects analysis with a Geisser-Greenhouse correction. Statistical analyses of tumor growth curves depicted in Figures 1B, 1C, and 5C were performed in R using a linear mixed-effects model analysis with the script detailed in Annex 1. p-values are depicted on the graphs in the figures of this manuscript.